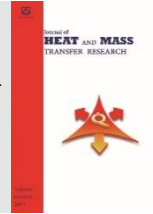




Semnan University



Research Article

Numerical Analysis of Solar Air Heater Roughened with B-Shape and D-Shape Roughness Geometry

Mayank Rautela ^a, Sohan Lal Sharma ^{*,b}, Vijay Singh Bisht ^a,
Ajoy Debbarma ^b, Rahul Bahuguna ^a

^a Department of Thermal Engineering, Faculty of Technology, Veer Madho Singh Bhandari Uttarakhand Technical University, Dehradun, 248007, U.K., India.

^b Department of Mechanical Engineering, National Institute of Technology, Hamirpur, 177005, H.P., India.

PAPER INFO

Paper history:

Received: 2023-05-21

Revised: 2023-08-29

Accepted: 2023-09-01

Keywords:

Solar air heater;
B-shape roughness;
D-shape roughness;
Nusselt number;
Friction factor;
Thermohydraulic performance.

ABSTRACT

A 2-D computational analysis of heat transfer augmentation and fluid flow characteristics with B-shaped and D-shaped artificial roughness has been carried out under the Reynolds number (Re) range from 4000-20000. Comparing the predictions of different turbulence models with experimental results available in the literature, the renormalization group k- ϵ (RNG) turbulence model is selected for the present study. A detailed analysis of heat transfer variation was done using various geometrical parameters such as four different pitch (P) values of 10, 15, 20, and 25 mm corresponding to pitch ratio (P/e) of 11.111, 16.666, 22.222, and 27.777 respectively, at constant height (e) of 0.9 mm. The highest value of Nusselt number (Nu) improvement reached up to 2.264 times and 21.91 times at P/e of 11.111 for B-shape and D-shape roughness respectively for Re of 20000 as compared to the smooth channel. A significant enhancement of heat transfer is predicted in the present simulation and the maximum Thermohydraulic Performance Parameter (THPP) attained up to 1.47 for B-shaped roughness. The novelty of the proposed model appears as present numerical findings offer better performance compared to existing research.

DOI: [10.22075/jhmtr.2023.30710.1445](https://doi.org/10.22075/jhmtr.2023.30710.1445)

© 2023 Published by Semnan University Press. All rights reserved.

1. Introduction

Energy seems in many forms but has one property in common, energy is possessed of the ability to generate a dynamic, vital effect. Coal, petroleum, natural gas, etc., are the source of conventional energy. Such energy sources are limited and soon will be drained with a growth rate of population, it is naturally occurring and takes much time, it cannot produce manually or by applying scientific methods. Non-conventional energy sources are non-polluted and the best alternative to conventional energy sources, it has increased at present time due to high environmental pollution. Solar energy is an essential source of renewable energy, and its use in natural form has also increased at a high rate, because it is a free source of

energy that is available almost throughout the year, especially in places near the equator. The renewable energy source has many advantages such as not emitting toxic and greenhouse gases, low maintenance cost, and helping in the electrification of rural areas. Tsoutsos et al. [1] presented an overview of the existing literature about the history, core principles, and recent advancements in the realm of solar thermal air heating systems. The discussion encompasses a range of solar collector designs, including evacuated tubes, flat plates, multiple passages, and cross-sectional flow passages. Wang et al. [2] studied and discussed the current situation and development of solar power in Tibet, China. According to their study, Tibet boasts abundant solar resources and holds

*Corresponding Author: Sohan Lal Sharma.

Email: sohansh@nith.ac.in

immense potential for the development of solar energy applications. Saidur et al. [3] conducted a study to examine the wind energy industry as per the wind energy policy. It was evident that an effective energy policy has the potential to enhance wind power generation and stimulate the overall energy industry. One of the important uses of solar energy is for space heating by solar air heaters (SAHs). In which the solar energy is captured by the absorber in the form of thermal energy to heat the flowing fluid i.e., air. This is especially useful in colder regions where the average environmental temperature is low and requires some external sources of energy to keep the homes and offices warm. It is the most effective technology out of all other solar technologies. SAH is simple in design, it requires less maintenance, doesn't require any external fuel to run, and does not pollute the environment. SAH is a device that absorbs the heat energy by the absorber plate which is given by the sun in the form of solar radiation and transfers this energy to the air flowing through the SAH channel. This cooled air is passed through the space to be kept warm. SAHs can be utilized in different places such as for space heating, timber seasoning, natural ventilation, drying of farm produce, paper mills, and industries for drying purposes. One of the major issues with SAHs is their poor thermal performance. This is because of the low convection coefficient between the absorber and flowing air. Different heat transfer enhancement techniques such as artificial roughness, turbulators, type of flow pass, etc., were employed to improve the performance of SAHs. Numerous experimental, numerical, and review research have been conducted to enhance the performance of SAHs in the past few years, some relevant works of literature are discussed in this section.

Goel et al. [4] conducted a thorough literature review on the history, fundamentals, and recent advancements in solar thermal air heating systems. It covers various designs of solar collectors, including evacuated tubes, flat plates, multiple passages, and cross-sectional flow passages, and analyzes and discusses them in detail. Dwivedi et al. [5] conducted a comprehensive summary of diverse literature sources, carefully compiled, and organized in their review. The focus of this review is to explore various methods utilized for enhancing the performance of solar air heating devices. The information is presented in a well-tabulated format, providing readers with an extensive overview of the subject. Sharma et al. [6] concentrated on various techniques such as artificial roughness, vortex generators, and thermal storage units, which are utilized to enhance the performance of SAHs. By implementing these methods, the thermal efficiency of the DPSAH was found to improve from 10% to 15% compared to the SPSAH. Furthermore, the integration of an absorber with a heat storage unit resulted in

further performance improvements. Chaurasia et al. [7] conducted a review to examine the utilization of two different roughness geometries (hybrid roughness) within a specified range of parameters and determine the optimal values that can enhance performance. The analysis focused on investigating the flow pattern resulting from the hybrid roughness. Prasad et al. [8] introduced a small-diameter wire as a roughness element to increase the thermal performance of SAH for the first time. Bopche et al. [9] studied and found that the rate of heat transfer between the absorber and the working fluid is negatively impacted by the viscous sub-layer. Turbulence within the air duct can improve the convection coefficient by depleting the laminar sub-layer, also the roughness causes friction to be lost. Consequently, the turbulence can only be produced in the laminar sub-layer, which is the area immediately surrounding the duct surface. Arulandam et al. [10] examined an unglazed absorber plate in a windless environment. Circular holes with a square pitch are part of the plate's geometry. The results of their research revealed that the low-conductive materials of absorbers can be used for better performance in low porosity and low flow scenarios. Chaube et al. [11] investigated the 2D computational domain of SAH to determine how utilizing various ribs in a rectangular duct would increase heat transfer and flow characteristics in turbulent flow regimes. They found that the result of the 2D model was closer to experimental findings than a three-dimensional model. They observed that the rectangular ribs with a surface area of $3 \times 5 \text{ mm}^2$ had the highest performance index. Chube et al. [12] performed a computational analysis to analyze the effectiveness of SAH using various types of ribs. In the event with rectangular ribs achieved the maximum heat transmission with the least amount of pressure loss at the ideal rib width. Continuous transverse ribs with chamfering exhibit a minor increase in heat transfer but a dramatic rise in friction factor. For constant pumping power conditions, rectangular ribs ($1 \text{ mm} \times 2 \text{ mm}$) had the best thermo-hydraulic performance when compared to all other types of ribs. Varol et al. [13] performed a numerical study on natural convection heat transfer in a flat and wavy absorber. The results revealed that the collector's form and inclination angle significantly affect fluid flow and natural convection heat transfer, and in every situation, wavy collectors provide better heat transfer than flat collectors. The maximum Rayleigh number for the largest inclination angle. This has been regarded as the most significant outcome of their numerical effort. Kumar et al. [14] numerically investigated the impact of arc-shaped geometry on thermohydraulic performance improvement in SAH ducts. For all the range of investigated parameters taken into consideration, $\alpha/90$ of 0.33 and e/D of 0.0426 yields the highest value of 1.7 for the gross

enhancement ratio. Karmare et al. [15] numerically analyzed the impact of circular, triangular, and square shapes rib grits on the performance of SAH with five different attack angles of 54°, 56°, 58°, 60° and 62° at $3600 \leq Re \leq 17000$. The Investigation revealed that a 58° angle of attack produced the best outcomes. Soi et al. [16] used K-shaped tabulators for the 2-dimensional flow analysis of SAH. The investigation demonstrated that the Nu grew as the Re number increased, and the highest value of Nu was found at P/e of 8.3. Rajput et al. [17] used square, triangular, rectangular, and chamfered tabulators to numerically evaluate the flow properties of SAH. They found that triangular and chamfered tabulators produced more heat transfer, whereas rectangular tabulators had the best overall performance index. Sharma et al. [18] examined the performance of SAH using square-shaped protrusion. They discovered that the highest Nu value was attained at the lowest P/e value. Gawande et al. [19] utilized circular-shaped tabulators in their numerical analysis and found that in every instance, the average Nusselt number grew along with a rise in the Reynolds number. For all the range of examined parameters, it was discovered that over the smooth duct, the friction factor increased by a maximum of 3.8 times corresponding to P/e of 7.14 and e/D of 0.042 were determined to match the optimum thermo-hydraulic performance of 2.03. Jhariya et al. [20] have done a numerical simulation of the 2-D model of a roughened SAH duct using semicircular transverse ribs as turbulators on the absorber plate. The maximum Nusselt number ratio of 2.4620, and the thermal performance factor of 1.33 corresponds to a relative roughness pitch (p/e) of 5 at a Reynolds number of 3800 was attained. Kumar et al. [21] conducted a computational study of solar air heaters with broken curved ribs, and they revealed that roughness configurations with a relative roughness pitch of 10 have a higher impact on the heat transfer augmentation of solar air heaters. Bisht et al. [22] used crown shape roughness to numerically analyze the thermohydraulic performance of SAH. Results reveal that the enhancement in Nusselt number and friction factor was obtained about 4.823 times and 1.937 times as compared to the smooth duct SAH. Ghildyal et al. [23] have carried out a comparative 2-dimensional study of solar air heaters with M-shaped, wedge-shaped, and reverse wedge-shaped roughness. They reported that M-shaped roughness elements have a higher value of thermohydraulic performance factor than the other two roughness. Bisht et al. [24] conducted a computational study of SAH roughened with V-shaped ribs and perforated V-shaped baffles. They reported that roughness orientation with a 24% open area ratio has a higher value of thermodynamic performance factor than other roughness combinations.

Bahuguna et al. [25] studied the economic performance of V-shaped ribs in SAH and found that roughness parameters and different cost factors of roughness have a large impact on life cycle savings. Similar strategies to raise the heat transfer using different novel inserts to augment the thermal performance of heat exchangers were also reported by various researchers like Bahuguna et al. [26], Chamoli et al. [27], Bahuguna et al. [28], Maithani et al. [29], and Bahuguna et al. [30]. Singh et al. [31] investigated the perforated multi-V ribs and continuous multi-V ribs and compared the effectiveness of SPSAH with these two types of ribs experimentally. Further, a study was expanded to examine the impact of perforation on these ribs in a parallel flow DPSAH, and it was observed that the perforated multi-V rib roughness offered the maximum value of THPP of 4.27. Singh et al. [32] experimentally analyzed the impact of changes in the open area ratio (β) on the performance of an SPSAH equipped with multi-V rib. When compared to the flat channel, the maximum enhancement in Nu, f, and THPP was recorded at approximately 6.33–8.19, 3.78–5.41, and 3.68–4.78 respectively. Singh et al. [33] conducted a comparative study on a parallel flow DPSAH roughened with continuous and perforated multi-V rib roughness. Comparison result reveals that the maximum enhancement in Nu, f, and THPP was found to be 5.93, 1.82, and 10.83 respectively over smooth duct SAH. Based on their earlier study mentioned above, Singh et al. [34] expanded their further study by providing a detailed discussion on the methodology and various steps involved in developing a correlation between variable parameters and the Nu and f for the parallel flow DPSAH. Sarreshtedari et al. [35] performed a numerical analysis to study the thermo-hydraulic characteristics of airflow over a 2-D ribbed channel having rib-width ratios ($B/H=0.5-1.75$) and spanned across different Re from 6000 to 18000. The study revealed that the THPP increased with higher Re. Additionally, a wider rib, indicating a higher B/H ratio, resulted in a reduced THPP. Noghrehabadi et al. [36] conducted an experimental study to analyze the performance of SAH under varying mass flow rates. The highest outlet temperature throughout the experiments reached about 77.1°C, while the peak thermal efficiency attained approximately 60%.

Gupta et al. [37] reviewed and summarized the ongoing research and development regarding the performance of solar water heaters that incorporate phase change materials and provide a viewpoint for future research and development in this field. Gupta et al. [38] reviewed and summarized ongoing research and development on the thermo-physical properties of SAHs and the effect of various roughness on heat transfer augmentation and provided a viewpoint for future research and development in this field. Karamveer et al. [39] conducted a detailed review to

assess the most preferable rib geometry for achieving maximum performance in a solar air heater. Among all the configurations considered, the multi-arc rib with gaps has been identified as the best configuration and exhibits the highest thermal efficiency, reaching approximately 79%. Karamveer et al. [40] conducted a case study on various performance parameters of an SAH to demonstrate the impact of different artificial roughness used in previous research. The best performance is observed at a $\Delta T/I$ higher than $0.00789 \text{ K}\cdot\text{m}^2/\text{W}$, with a unique combination of parameters such as $P/e = 10$, $e/D_h = 0.043$, and $\alpha = 600$. Karamveer et al. [41] incorporated Multiple Open Trapezoidal Ribs (MOTR) to take advantage of heat transfer enhancement through secondary flows in their experimental work. The experiment's results reveal that at $P/e = 10$, $L/w = 0.8$, and $e/D_h = 0.043$, the Nu exhibits the highest augmentation, being 6.05 times greater compared to the smooth absorber plate. Furthermore, an evaluation of the THPP yielded values ranging from 3.24 to 3.79.

Gupta et al. [42] presented an experimental investigation of an artificially roughened solar air heater with MOTR roughness with the gap. The maximum value of Thermo-hydraulic performance parameters (THPP) achieved in the experiments reached up to 3.99. In addition, correlations for the Nusselt number and friction factor were developed based on the experimental data. In their further study, Karamveer et al. [43] developed the empirical correlations for Nu and f and demonstrated the significant increase in the Nu compared to a smooth absorber plate, with the highest augmentation observed at 6.07 times. Furthermore, these correlations exhibit a high level of accuracy, with an average absolute deviation of 5.47% for Nu and 5.02% for the friction factor (f). Gupta et al. [44] performed an experimental investigation examining the effect of P/e on heat transfer and flow friction in an artificially roughened SAH for Re ranging between 2000 and 16000. The result reveals that the $P/e = 10$ exhibits a higher level of heat transfer augmentation as well as a higher pressure penalty over other P/e values.

Table 1 explains the comparison of different roughness geometries chronologically to give the audience an idea about the development of roughness work in rectangular duct SAHs.

The available literature reveals that researchers have employed a variety of artificial roughness including grooves, dimples, protrusions, fins, ribs, baffles, winglets, and hybrid roughness to enhance the performance of SAHs. The B-shape, and D-shape roughness on the absorber has never been considered in previous literature.

Therefore, the main aim of the current study is to improve heat transmission and thermal performance

of SAH using B-shape and D-shape roughness geometry under varying Reynolds numbers. Both B shape and D shape roughness elements in SAH play crucial roles in augmenting heat transfer performance. The selection of B shape and D shape roughness geometry can be justified by their proven abilities to disrupt the laminar boundary layer, induce turbulence, delay flow separation, and promote better mixing of air near the heated surface for efficient heat transfer. Wood et al. [83] performed an experimental and numerical analysis to study the flow behavior of smooth and rigid hemisphere-type roughness.

The result revealed that the curved obstacles (like sphere, hemisphere, B, and D shape geometries) form wake formation at the far side of the flow that generates turbulence in a large flow area. The flow over a curved obstacle accelerates over its top surface, and at the back of the obstacle recirculation of flow takes place that disturbs the main flow effectively.

The arrangements of the B shape and D shape roughness in a uniform manner create effective turbulence with low frictional pressure drop. That's why these roughness geometries are considered for the present study. These geometries have demonstrated superior performance in empirical studies when compared to other roughness geometries, making them reliable choices for enhancing the overall thermal efficiency of the SAH.

1.1. Novelty and Objective

The novelty of the B-shape and D-shape roughened SAH duct lies in their distinct roughness geometries, which set them apart from other roughness geometries. Compared to traditional roughness geometries such as fins, baffles, dimples, protrusion, winglets, V-shape, W-shape roughness, etc., the B-shape and D-shape configurations offer unique advantages in terms of flow manipulation and heat transfer enhancement. A 2-D CFD model of single-pass SAH roughened with these geometries (B shape and D shape) under various geometrical and flow conditions has been considered to analyze thermohydraulic performance, which is novel in fashion.

The main objective of the present study is to investigate the impact of B-shape and D-shape rib roughness on heat transfer, frictional losses, and fluid flow properties of SAH, and to obtain sufficient data for the researchers, and potential users.

The purpose of this study is to learn how the variation of pitch ratio affects the heat transfer and fluid flow characteristics at constant roughness height.

Table 1. Comparison of different roughness geometries used in rectangular duct SHAs

Authors (Yrs.)	Roughness Type	Optimized Parameters	Optimal Results	Key Findings
Bopche et al. [9]	U-shape ribs (Inverted)	$P/e = 10$, $e/D_h = 0.0398$,	$Nu/Nu_s = 2.82$, $f/f_s = 3.72$, THPP = 1.82	Inverted-U-shaped ribs were shown to be more efficient than wedge-shaped ribs and dimple-shaped turbulators.
Bhushan et al. [45]	Hemispherical turbulators	$L/e = 31.25$, $d/D_h = 0.294$,	$Nu/Nu_s = 2.8$, $f/f_s = 2.2$,	Present roughness shows a more significant increase in the rate of heat transfer over the smooth channel.
Lanjewar et al. [46, 47]	W-shape ribs	$P/e = 10$, $e/D_h = 0.0337$, $\alpha = 60^\circ$ $Re = 6000$	W-down ribs $Nu/Nu_s = 2.36$, $f/f_s = 2.01$, THPP = 1.99, W-up ribs $Nu/Nu_s = 2.24$, $f/f_s = 2.35$, THPP = 1.81	W-shaped ribs were shown to be more effective than V-shaped roughness in the parametric range, and the frictional losses decreased for an attack angle below 60° .
Kumar et al. [48]	V-shape ribs with space	$P/e = 10$, $e/D_h = 0.043$, $\alpha = 60^\circ$	THPP = 1.6	The numerical approach was determined to be 6.25 times more efficient than the conventional method.
Yadav et al. [49]	Angular arc of the circular protrusion	$P/e = 12$, $e/D_h = 0.03$, $\alpha = 60^\circ$	$Nu/Nu_s = 2.89$, $f/f_s = 2.93$	The proposed roughness improves heat transmission over the baseline model for the range of investigated parameters.
Karwa et al. [50]	60° V-down discrete ribs	$P/e = 10.63$, $e/D_h = 0.047$, $\alpha = 60^\circ$ $Re = 11150$	$\eta_{th} = 12.5$ to 20%	The rate of heat transmission was improved at lower flow rates.
Singh et al. [51]	Multiple arc ribs	$P/e = 8$, $e/D_h = 0.045$, $\alpha = 60^\circ$, $Re = 22,300$	$Nu/Nu_s = 5.07$, $f/f_s = 3.71$,	The heat transfer rate escalates with an increase in Re , understudied parameters.
Yadav et al. [52]	Equilateral triangular shape ribs	$P/e = 7.14$, $e/D_h = 0.042$, $Re = 15000$	$Nu/Nu_s = 3.073$, $f/f_s = 3.356$, THPP = 2.11	The optimal enhancement of Nu was obtained at a higher Re , while the highest f was obtained at a lower Re (3,800).
Maithani et al. [53]	V-rib with similar space	$P/e = 10$, $e/D_h = 0.0431$, $Re = 6000$	$Nu/Nu_s = 2.59$, $f/f_s = 2.87$, THPP = 1.43	Space between V-ribs induces a secondary fluid motion. This secondary flow is likely to interact with the primary flow, leading to heightened turbulence and subsequently enhancing heat transfer.
Pandey et al. [54]	Multiple arcs with space	$P/e = 8$, $e/D_h = 0.044$, $\alpha = 60^\circ$, $Re = 21000$	$Nu/Nu_s = 5.85$, $f/f_s = 4.96$, THPP = 3.6	A uniform air mixing was obtained at $W/w = 5$. The present roughness enables a higher heat transfer enhancement of up to 585% over the plain duct.
Gawande et al. [55, 56]	Chamfered ribs	$P/e = 7.14$, $e/D_h = 0.042$, $\alpha = 20^\circ$, $Re = 15000$	$Nu/Nu_s = 3.247$, $f/f_s = 3.835$, THPP = 2.047	By varying the chamfer angle from 0 to 10, the heat transfer was enhanced by 11.23%, and the maximum efficiency was reached about 70%.
Bhardwaj et al. [57]	Inclined ribs	$P/e = 12$, $e/D_h = 0.043$, $\alpha = 60^\circ$, $Re = 18000$	$Nu/Nu_s = 3.13$, $f/f_s = 2.96$, THPP = 4.376	N/A
Sawhney et al. [58]	Wavy-delta wings	$P/H = 3$, $\theta = 5^\circ$, $Re = 4000$	$Nu/Nu_s = 2.23$, $f/f_s = 10.3$, THPP = 2.09	The heat transmission performance was obtained about 223% higher for the present geometry as compared to the plain duct.
Gabhane et al. [59]	C-shape ribs (multiple)	$P/e = 24$, $e/D_h = 0.02$, $\alpha = 90^\circ$, $Re = 15000$	THPP = 3.048	N/A
Kumar et al. [60]	Rectangular ribs	$P/e = 10$, $e/D_h = 0.04$, $e/w = 4$, $Re = 15000$	$Nu/Nu_s = 2.37$, $f/f_s = 4.5$, THPP = 1.89	The highest heat transmission improvement was obtained at $e/w = 4$, and 44% more efficient over $e/w = 0.25$.
Alam et al. [61]	Conical shape turbulators	$P/e = 10$, $e/D_h = 0.044$	$Nu/Nu_s = 2.3$, $f/f_s = 5.43$, THPP = 1.35	The present mathematical model is 1.35 times more efficient as compared to the base model, and thermal efficiency reached about 70%.
Thakur et al. [62]	V-shape ribs	$P/e = 10$, $e/D_h = 0.03$, $\alpha = 60^\circ$, $Re = 6000$	THPP = 2.3	V-shape ribs offered superior performance as compared to the inclined roughness for the given range of operating parameters.

Singh et al. [63]	Square wave transverse ribs	$P/e = 10$, $e/D_h = 0.043$, $Re = 15000$	$Nu/Nu_s = 2.14$, $f/f_s = 3.55$, $THPP = 1.43$	Analytical investigation revealed that the non-uniform cross-section ribs were more efficient than uniform cross-sectional ribs.
Kumar et al. [64]	Twisted ribs	$P/e = 8$, $y/e = 3$, $\alpha = 60^\circ$	$Nu/Nu_s = 2.58$, $f/f_s = 1.78$, $THPP = 2.13$	$\alpha = 90^\circ$ and the $y/e = 7$ offers an optimum value of friction factor.
Soi et al. [65]	Semi-hemispherical turbulators	$w/W = 0.166$, $e/D_h = 0.036$	$Nu/Nu_s = 3.9$, $f/f_s = 1.8$	The highest value of Nu and f was obtained at about 232, and 0.019 respectively under a specified range of operating parameters.
Abuska [66]	Conical shape	N/A	$m = 0.1$	The maximum thermal efficiency was obtained at about 74.6%, at $m = 0.1$ kg/sec, and strongly depends on the type of roughness and the intensity of radiation.
Debnath et al. [67]	Pentagonal ribs	$P/e = 8$, $e/D_h = 0.045$, $Re = 38414$	N/A	An analytical study revealed that heat transfer enhancement occurs by increasing the P/e value and decreasing the value of e/D_h . And the reverse trend was followed for f .
Singh et al. [68]	Multiple broken transverse ribs	$P/e = 10$, $e/D_h = 0.043$, $Re = 15000$	$Nu/Nu_s = 3.24$, $f/f_s = 3.85$, $THPP = 2.1$	The maximum thermal and effective efficiency obtained was approximately 72.25% and 69.15% respectively.
Bezbaruah et al. [69]	Half conical turbulators	$\alpha = 60^\circ$, $Re = 5000$	$THPP = 1.06$	The THPP of half conical VG was superior to the truncated conical VGs for $3000 \leq Re \leq 10000$.
Kumar et al. [70]	Multi-arc ribs (discrete)	$d/x = 0.6$, $g/e = 1$, $N_g = 3$, $Re = 19000$	$THPP = 1.6$	The ANOVA technique for the present study revealed that the discrete multiple arc rib was 483% more efficient than the plain duct.
Wang et al. [71]	Curved ribs	$P/e = 20$, $g/e = 1.5$, $W/w = 4$, $Re = 19258$	$Nu/Nu_s = 5.42$, $f/f_s = 5.87$	The optimum thermal efficiency was obtained at about 65%, and the pressure drops varied from 15.8 to 30 Pa.
Kumar et al. [72]	Curved ribs	$g/e = 1$, $W/w = 3$, $d/x = 0.65$ $\alpha = 60^\circ$	N/A	The highest value of Nu with rib gap was obtained about 358, and rib space accelerates the fluid flow, resulting in an improved distribution of local Nu .
Ahmad et al. [73]	Prism type ribs	$P/e = 28.57$, $e/D_h = 0.0167$, $Re = 4000$	$Nu/Nu_s = 4.99$, $f/f_s = 3.71$, $THPP = 3.41$	For the present roughness, the lowest value of pressure drops reached 2.13 times as compared to the plain duct for the specified range of operating parameters.
Ngo et al. [74]	Multiple conic curve-type ribs	$P/e = 10$, $e/D_h = 0.03$, $Re = 8000$	$Nu/Nu_s = 1.93$, $f/f_s = 2.04$, $THPP = 1.56$	The highest Nu and the lowest value of f were observed at about 52.2, and 0.017 at $K = -4$ (hyperbola).
Rathor et al. [75]	Inclined ribs with space	$P/e = 10$, $e/D_h = 0.0303$, $\alpha = 60^\circ$, $Re = 12438$	$Nu/Nu_s = 3.29$, $f/f_s = 4.04$, $THPP = 2.06$	The heat transfer improved by 329% using present roughness as compared to the plain duct, and the LCT method was adopted for temperature measurements.
Mahanand et al. [76]	Inverted T-shape ribs	$P/e = 7.14$, $e/D_h = 0.042$, $Re = 15000$	$Nu/Nu_s = 2.747$, $f/f_s = 3.404$, $THPP = 1.87$	For a higher mass flow rate, the inverted T-ribs were more efficient than circular ribs.
Mahanand et al. [77]	Quarter circular ribs	$P/e = 7.14$, $e/D_h = 0.042$, $Re = 15000$	$Nu/Nu_s = 2.774$, $f/f_s = 3.435$, $THPP = 1.88$	Under the selected range of operating parameters, the lowest f value of 3.22 times was attained than the plain duct.
Jain et al. [78]	Arc shape ribs with multiple spaces	$P/e = 10$, $e/D_h = 0.043$, $N_g = 3$, $Re = 18000$	$Nu/Nu_s = 3.74$, $f/f_s = 2.69$, $THPP = 2.75$	The rate of heat transmission and f has been improved by approximately 274% and 169% respectively at $N_g = 3$ for present roughness geometry.
Azad et al. [79]	Discrete arc ribs	$P/e = 10$, $e/D_h = 0.045$, $\alpha = 30^\circ$, $Re = 14000$	$Nu/Nu_s = 2.26$, $f/f_s = 3.87$, $THPP = 1.68$	The present mathematical model using MATLAB revealed that the proposed geometry was more efficient than novel V-ribs.
Bhuvad et al. [80]	Apex-up discrete ribs	$P/e = 10$, $e/D_h = 0.045$, $\alpha = 30^\circ$, $Re = 10000$	$Nu/Nu_s = 2.92$, $f/f_s = 3.04$, $THPP = 2.01$	The present roughness geometry was found to be more efficient than the apex-down arc rib configuration.
Arya et al. [81]	V-shape miniature with dimples	$l/d = 20$, $e/D_h = 0.036$, $S/d = 15$, $\alpha = 45^\circ$, $Re = 20000$	$THPP = 1.73$	After the comparative study, it was observed that the THPP of dimples with V-rib miniature was about 1.2 times higher than pure dimples.
Arya et al. [82]	Dimples with various shapes miniature	$l/D = 20$, $w/D_h = 0.18$, $\alpha = 45^\circ$, $Re = 12500$	$THPP = 1.63$	The maximum THPP = 1.63, was obtained using dimples with V-miniature as compared to the dimples with another miniature shape.

2. Analysis of the Numerical Model

To determine how the performance of SAH will change, a 2-dimensional numerical investigation has been carried out using a new type of roughness geometry. As compared to the 3-D model, the 2-D model requires fewer computational resources in terms of memory, processing power, and time during simulations. This makes 2D simulations more computationally efficient, allowing for faster calculations and analysis. Transverse ribs generate almost negligible secondary flow, hence the 2D model may predict the same outcomes as the 3D model proposed and compared by Chaube et al. [84]. The 2D model is preferred as compared to the 3D model to reduce the calculation time for the simulation. B-shape and D-shape tabulators were employed in this study to thermohydraulic performance of SAH. The analysis for each roughness was done at four different pitch distances 10 mm, 15 mm, 20 mm, and 25 mm (for pitch ratio of $P/e = 11.111, 16.666, 22.222, \text{ and } 27.777$) at constant width of roughness ($e = 0.9 \text{ mm}$). In this analysis, the computational domain of SAH was created similarly to Chaube et al. [84]. For the design of the 2-D flow domain, the ASHRAE standard 93-2003 [85] guidelines were utilized. The schematic diagram of the 2-D CFD model of SAH and the present roughness geometry, B-shaped and D-shaped roughness is done in ANSYS software in space claim as explained in Figure 1 (a) and (b) respectively.

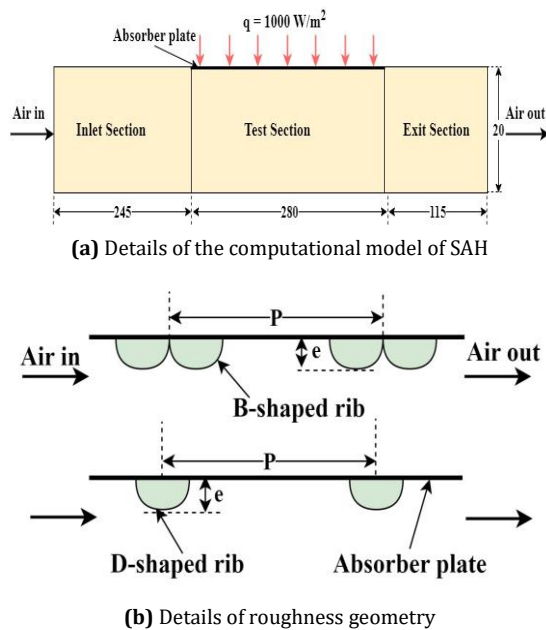


Figure 1. Schematic diagram of computational model and roughness geometry

2.1. Computational Domain and Operating Parameters of Roughened SAH

A computational model of the Solar Air Heater (SAH) duct is developed using ANSYS (Fluent). The

SAH flow domain consists of B-shaped and D-shaped tabulators with varying pitch distances. The computational model is divided into three parts: the entry section, the test section, and the exit section. The total length of the duct (L) is 640 mm, and its height (H) is 20 mm. The inlet and outlet sections have dimensions of 245 mm and 115 mm, respectively. The test section, where the absorber plate is located, measures 280 mm in length and 100 mm in width. The hydraulic diameter of the rectangular duct is 33.33. The absorber plate contains different tabulators and a fixed heat flux of $I = 1000 \text{ W/m}^2$ is applied on it.

For this numerical simulation, the pitch distance (P) for B shape and D shape roughness varies from 10 mm to 25 mm (five values), and a constant rib height (e) of 0.9 mm is used. The pitch distance is taken as 10 mm, 15 mm, 20 mm, and 25 mm corresponding to the pitch ratio (P/e) of 11.111, 16.666, 22.222, and 27.777 respectively. For the present study, the recommendations for rib height by Verma et al. [86] are utilized and expressed below:

If $e \ll \delta'$, roughness has no impact on the characteristics of the flow.

If $e \gg \delta'$, there will be a greater pressure drop than an increase in heat transfer.

If $e \geq \delta'$, a good amount of heat transfer increased with a moderate pressure drop.

The working fluid used is ambient air, introduced at an inlet temperature of 300K. Table 2 provides a detailed list and range of the geometrical and operating parameters. To validate the obtained results of heat transfer from the present CFD simulation for smooth ducts, a comparison is made with the theoretical correlations. The ANSYS software greatly reduces the computation time by reducing the number of variables, resulting in a more efficient calculation process. This leads to significant time and resource savings. The main assumptions for numerical simulation are as follows:

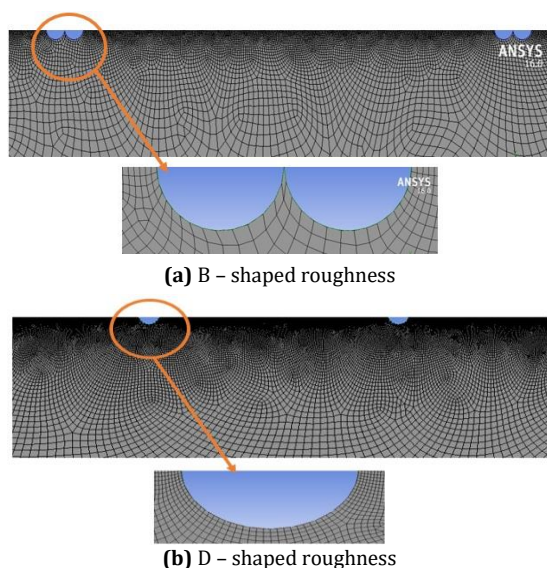
- Consistent flow.
- Zero pressure fluctuation in the y-direction.
- There is no shear force in the y-direction.
- Gravitational body force has been disregarded.
- Incremental flow.
- The flow has been fully generated at the test section's inlet.
- The fluid's axial heat conduction was minimal.
- Atmospheric pressure and temperature of air remain constant.

Table 2. Dimensional details of computational domain and roughness geometry

Boundary condition	Values
Duct total length (L)	640 mm
Entrance section length (L_1)	245 mm
Test section length (L_2)	280 mm
Exit section length (L_3)	115 mm
Duct width (W)	100 mm
Duct height (H)	20 mm
Roughness ribs height (e)	0.9 mm (fixed)
Rib pitch (P)	10 mm, 15 mm, 20 mm, and 25 mm
Hydraulic Diameter (D_h)	33.33 mm
Pitch ratio (P/e)	11.111, 16.666, 22.222, and 27.777
Height ratio (e/D_h)	0.027 (fixed)
Heat Flux (I)	1000 W/m ² (fixed)
Reynolds number range	4000, 8000, 12000, 16000, and 18000
Inlet Temperature of air	300K

2.2. Grid Generation and Grid Independence Test

One of the most important features is the fact that CFD software like ANSYS finds flow properties at specific points rather than calculating them across the entire domain. To accomplish this, meshing must be used to split the entire domain into a variety of cells and nodes because it reduces the calculation to a very low level. Utilizing CFD software, the flow characteristics at these specific nodes will be calculated. With more nodes created, the accuracy of the outcome will rise. In this case, a structural quadrilateral meshing is used. To achieve uniform meshing, a 0.2 mm body size and face meshing is used. Figure 2 (a), and (b) represent the meshing of B-shape and D-shape roughness geometry.

**Figure 2.** Meshing of present roughness geometry.

As per the discussion from the previous studies, the results for flow properties become more precise as the number of nodes increases. But it also lengthens the amount of time needed to calculate the results. To evaluate the impact of flow properties the number of nodes in the fluid domain increased continuously during the simulation. The Nu is one of the characteristics utilized in the analysis of heat transfer. As the number of nodes is raised, the Nu will increase. However, at a threshold point where increasing more nodes will only result in a small increase in the Nu. As a result, the process of adding more nodes will be stopped to avoid wasting computational time. For the present simulation, the Nu increases at a very slow rate after 320000 cells, as can be seen in Table 3. Therefore, the number of cells at 329806, and perform additional calculations using this number of cells.

Table 3. Grid independency test

S. NO.	Total nodes	Total cells	Nusselt number
1	295762	12536	78.76
2	682531	221832	93.88
3	928155	310128	107.69
4	987398	329806	114.78
5	1012157	348325	114.95

2.3. Governing Equations Used for Heat Transfer and Fluid Flow Analysis

The software needs some governing equations after meshing is finished to identify the specific solution. The governing equations are preinstalled in CFD software like ANSYS (Fluent). The software will output the results after, only inputting the boundary conditions and choosing the governing equation. As previously mentioned, the governing equations in the ANSYS software are chosen by selecting one of the available uneven air movement models, such as the k- ϵ model, k- ω model, etc. In our analysis, the k- ϵ model, which employs the renormalization group sub-method, was used. The following governing equations are used in this model.

Continuity Equation

The continuity equation is the mathematical representation of the principle of mass conservation as applied to an elemental control volume within a fluid in motion, and is given by:

$$\frac{\partial \rho}{\partial t} + \frac{\partial(\rho u)}{\partial x} + \frac{\partial(\rho v)}{\partial y} + \frac{\partial(\rho w)}{\partial z} = 0 \quad (1)$$

Momentum Equation

It is based on the law of conservation of moment or on the momentum principle for turbulent flow field, which states that the net force acting on a mass

acceleration fluid is equal to the change in momentum of flow per unit of time in the direction.

$$\frac{\partial}{\partial x_j}(\rho u_i u_j) = -\frac{\partial p}{\partial x_i} + \frac{\partial}{\partial x_j} \left[\mu \left(\frac{\partial u_i}{\partial x_j} + \frac{\partial u_j}{\partial x_i} \right) \right] - \frac{\partial}{\partial x_j}(\rho u'_i u'_j) \tag{2}$$

Energy equation

$$\frac{\partial}{\partial x_i}(u_j(\rho e + p)) = \frac{\partial}{\partial x_j} \left[\lambda \frac{\partial T}{\partial x_j} \right] \tag{3}$$

Renormalization Group (RNG) k- ε Model

$$\frac{\partial(\rho k)}{\partial t} + \frac{\partial(\rho k u_i)}{\partial x_i} = \frac{\partial}{\partial x_j} \left[\frac{\mu}{\sigma} \frac{\partial k}{\partial x_j} \right] + 2\mu_i E_{ij} E_{ji} - \rho \epsilon \tag{4}$$

$$\frac{\partial(\rho \epsilon)}{\partial t} + \frac{\partial(\rho \epsilon u_i)}{\partial x_i} = \frac{\partial}{\partial x_j} \left[\frac{\mu}{\sigma_\epsilon} \frac{\partial \epsilon}{\partial x_j} \right] + C1 \epsilon \frac{\epsilon}{k} 2\mu_t E_{ij} E_{ji} - C2 \epsilon \rho \frac{\epsilon^2}{k} \tag{5}$$

$C_{\mu} = 0.09, \quad \sigma_k = 1.00, \quad \sigma_\epsilon = 1.30, \quad C1_\epsilon = 1.44, \quad C2_\epsilon = 1.92$

Due to good thermo-physical properties, machinability, high thermal conductivity, low weight, and low cost, the ribs in this study are made of solid aluminum, and air is a working fluid. The properties of absorber material and air are listed in Table 4.

Table 4. Thermophysical properties of Aluminum and air

Properties	Aluminum	Air
Specific heat (Cp)	871 J/kgK	1006.4 J/kgK
Density (ρ)	2719 kg/m3	1.1760 kg/m3
Thermal conductivity (k)	202.4 W/mK	0.02624 W/mK
Dynamic viscosity (μ)	-	1.857× 10 ⁻⁵ kg/ms

The values of specific properties must be applied at specific points for the CFD software to begin calculating the values of those properties at those nodes (such as at the inlet and absorber plate, etc.). The properties at other nodes are then determined using interpolation. This allows us to find properties across the entire domain and find average properties where they are required. A uniform heat flux of I=1000 W/m2 on the absorber plate. (This is the solar insolation falling on the absorber plate). No-slip condition in ANSYS (Fluent) is specified at the walls to compute the air velocity, and zero-stress wall boundary conditions are used throughout the rectangular duct to achieve the desired outcomes. The turbulent intensity is assumed to be 5% for the present simulation.

3. Result and Discussion

A variety of findings from the CFD analysis of the roughened solar air heater are discussed in this section. With the aid of the ANSYS (Fluent) results, the characteristics of heat transmission, pressure drop, friction factor, turbulent kinetic energy, temperature change, and energy conversion are observed and discussed. With the inclusion of other turbulators, these results will change. The thermo-hydraulic performance factor will be used to compare all findings at the end. In this study, Reynolds number (Re) ranges from 4000 to 18000, and the pitch (P) is varied from 10 mm, 15 mm, 20 mm to 25 mm, corresponding to a pitch ratio of (P/e = 11.111, 16.666, 22.222 and 27.777) at constant roughness height (e) of 0.9 mm corresponds to height ratio (e/D_h) of 0.027, and the hydraulic diameter (D_h) of 33.33 mm.

3.1. Validation of Turbulence Model with Standard Correlations

The present CFD analysis findings were compared to the correlations of Nusselt number (Nu) and friction factor (f) derived from the Dittus-Boelter equation by Kays et al. [87] and Blasius equation by Bhatti et al. [88], respectively. The results of the CFD analysis for smooth duct were compared to the predictions obtained from the Dittus Boelter correlations for Nu and the Blasius correlation for f. This allowed for a comprehensive evaluation of the accuracy and applicability of the present CFD model in predicting heat transfer and friction characteristics.

Dittus-Boelter [87]

$$Nu_s = 0.023 * Re^{0.8} * Pr^{0.4} \tag{6}$$

Blasius correlations [88]

$$f_s = 0.085 * Re^{-0.25} \tag{7}$$

The CFD analysis results were compared to empirical correlations to assess their accuracy. The percentage error between the Nu and f values obtained from the numerical study and the empirical correlations were found to be ±10% and ±13% respectively. The variation of Nu and f concerning Reynolds number (Re) is illustrated in Figure 3. The figure demonstrates that both the numerical study and empirical correlations yield nearly equal results with good agreement. This indicates that the numerical solution provides the correct values for the desired outcomes. Therefore, the CFD analysis is deemed suitable for obtaining the desired results in the present study. The effect of roughness pitch and Re on various thermal and thermohydraulic parameters are discussed as follows:

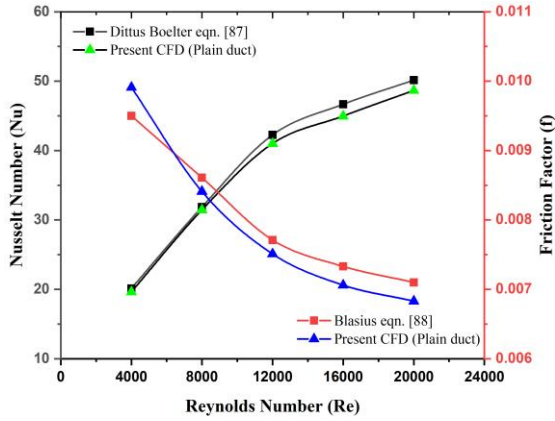
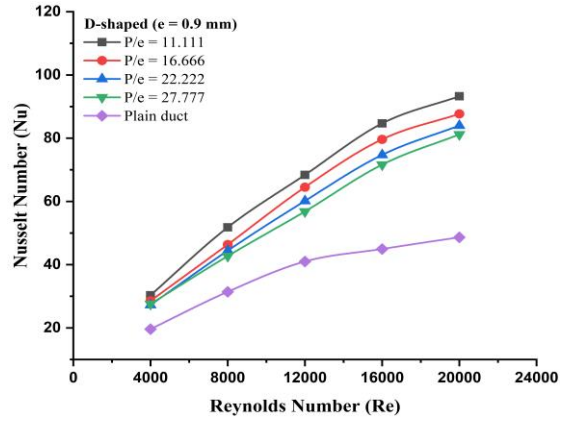


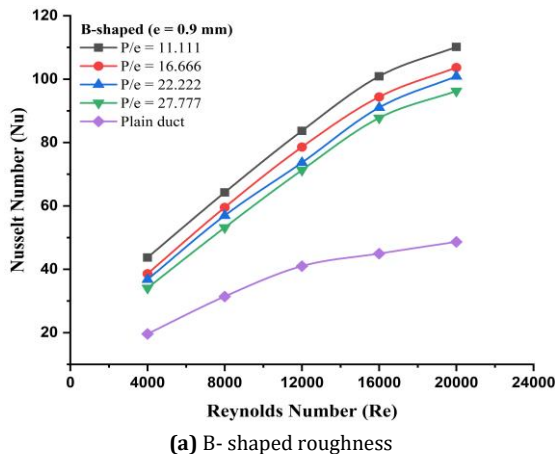
Figure 3. Validation of Nu and f for a smooth duct with standard correlations



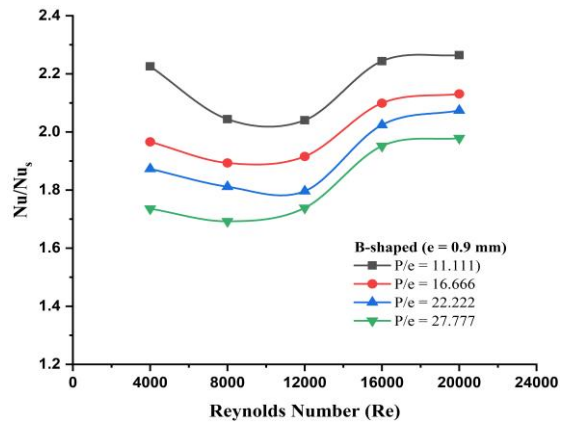
(b) D- shaped roughness
Figure 4. Variation of Nu with Re

3.2. Effect on Heat Transfer Characteristics

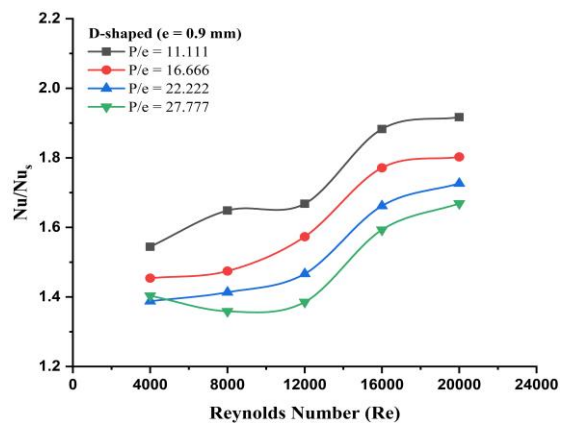
Here, a numerical analysis of the SAH is executed to determine the improvement in heat transmission. To improve heat transfer in this investigation, two different types of ribs such as B and D-shaped ribs were used. Since all other variables are held constant, Re is the major factor in determining the performance of SAH. Figure 4 (a) and (b) represent the variation of the Nu concerning the Re in the SAH duct having B shape, and D shape roughness respectively for fixed rib height (e) of 0.9 mm and different roughness pitch (P) values of 10 mm, 15 mm, 20 mm, and 25 mm, corresponding to a pitch ratio (P/e) value of 11.111, 16.666, 22.222 and 27.777 respectively. The roughness pitch, which refers to the gap between two successive ribs, plays a crucial role in enhancing heat transfer. The results show that as the Re increases, the average Nu also increases, indicating improved heat transfer. The enhancement in heat transfer is more significant at higher Re (20,000) compared to lower values (Re = 4,000) when compared to the smooth duct. Lower roughness pitch values result in higher Nu, indicating more effective heat transfer. On the other hand, increasing the roughness pitch reduces the heat transfer rate. This can be attributed to the increased number of ribs in the test section for a lower roughness pitch, which generates greater turbulence compared to configurations with a higher roughness pitch. The highest value of Nu was obtained about 110.15, and 93.25 for B shape and D shape roughness respectively for P/e of 11.111 at higher Re of 20000.



(a) B- shaped roughness



(a) B- shaped roughness



(b) D- shaped roughness

Figure 5 (a), and (b) illustrates the effect of relative roughness pitch (P/e) on heat transfer in a B shape and D shape rib-roughened duct respectively, represented as the ratio of the Nu enhancement (Nu/Nu_s) for the roughened duct to that for a smooth duct. The Nu/Nu_s increases with Re, ranging from 4,000 to 20,000. Notably, the ratio has a higher value of 2.26 times and 1.92 times for B shape and D shape configurations respectively with a low relative roughness pitch of 11.111 at Re of 20000.

Figure 5. Variation of Nu/Nu_s with Re

3.2.1. Temperature Contour

The temperature contours obtained from the numerical analysis illustrate that the roughness elements affect the temperature distribution. Higher temperatures are typically observed in regions where the roughness elements are present, indicating increased heat transfer. The contours also show the flow patterns and how heat is transferred from the absorber plate to the air flowing through the heater. Figure 6 (a), (b), (c), and (d) use a B-shaped roughness to show the temperature change inside a flow duct. This graph is created using the Reynolds number of 18000. The air's inlet temperature is 300K. The duct's interior can reach a maximum temperature of 328.296K at $P = 10$ cm ($P/e = 11.111$).

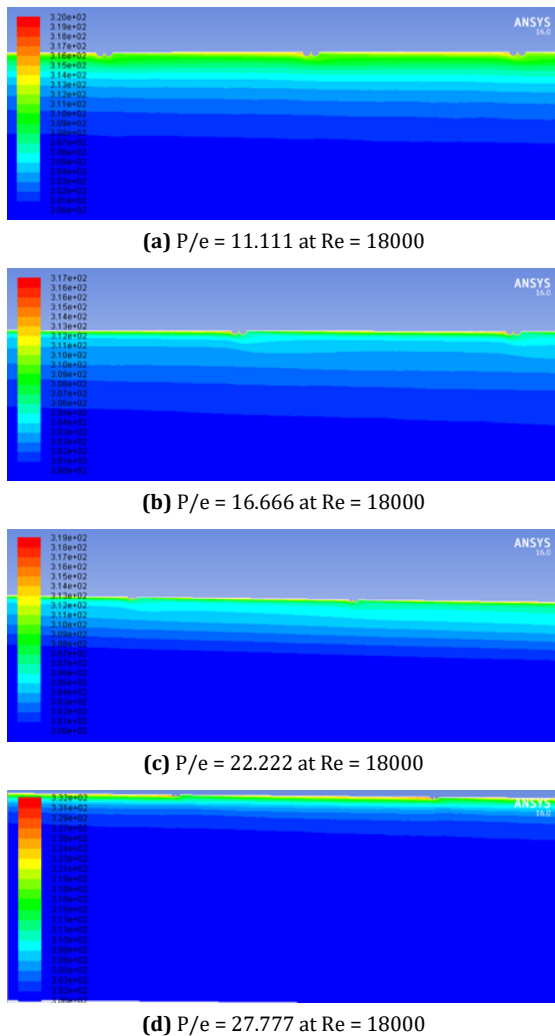


Figure 6. Temperature contours of B-shaped roughened SAH at Re 18000

Figure 7 (a), (b), (c), and (d) use a D-shaped roughness to show the temperature change inside a flow duct. This graph is created using the Reynolds number of 18000. The air's inlet temperature is 300k. The duct's interior can reach a maximum temperature of 314.295K at $P = 10$ cm ($P/e = 11.111$).

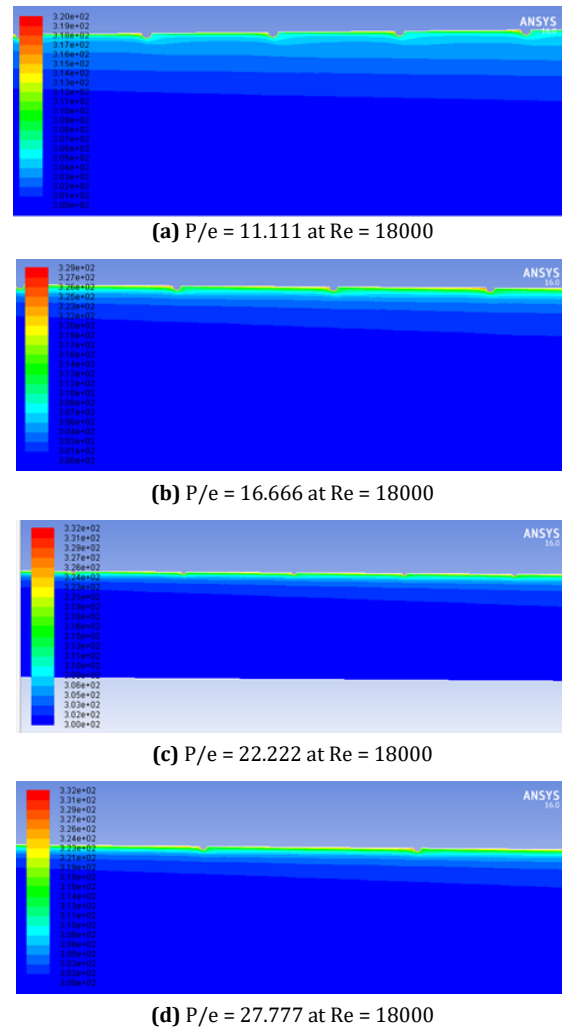
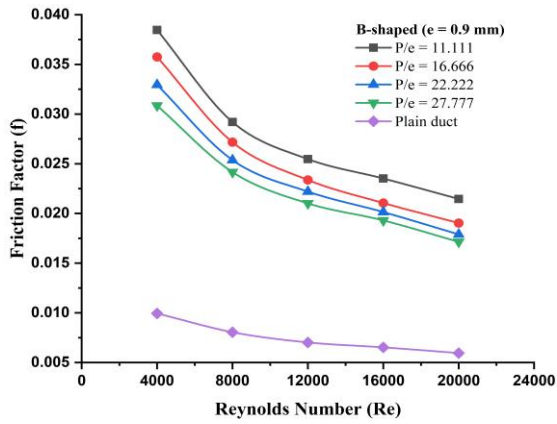


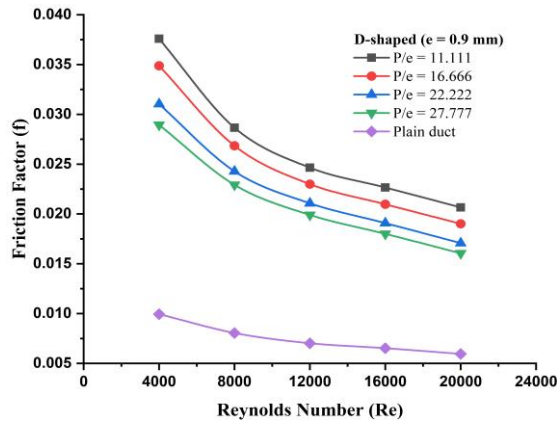
Figure 7. Temperature contours of D-shaped roughened SAH at Re 18000

3.3. Effect on Frictional Characteristics

Figure 8 (a), and (b) depicts the relationship between the average friction factor (f) and Reynolds number (Re) of roughened SAH duct having B shape and D shape roughness respectively for fixed rib height (e) of 0.9 mm and different roughness pitch (P) values of 10 mm, 15 mm, 20 mm, and 25 mm, corresponding to a pitch ratio (P/e) value of 11.111, 16.666, 22.222 and 27.777 respectively. The friction factor in a roughened duct is significantly higher compared to a smooth duct. The results show that the friction factor has a more pronounced effect at low Re (4,000). As the Re increases from 4,000 to 20,000, the f decreases. This trend can be attributed to the presence of more obstructions (B shape and D shape roughness) in the flow field with a low P/e of 11.111. These obstructions increase the resistance to flow, resulting in higher friction factors. In contrast, high P/e configurations have fewer obstructions, leading to lower friction factors. The higher value of f was obtained about 0.038 and 0.0266 for B shape and D shape configuration respectively at $P/e = 11.111$, and Re of 4000 as compared to the smooth duct.



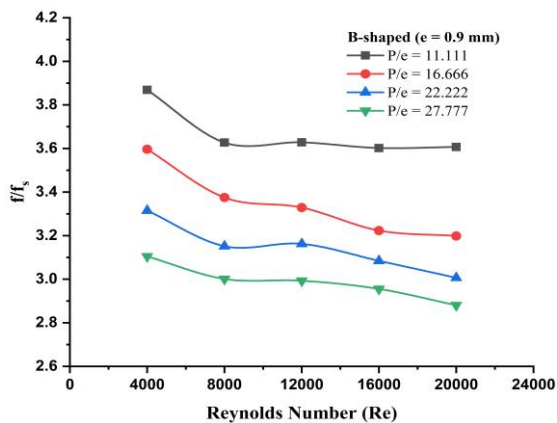
(a) B-shaped roughness



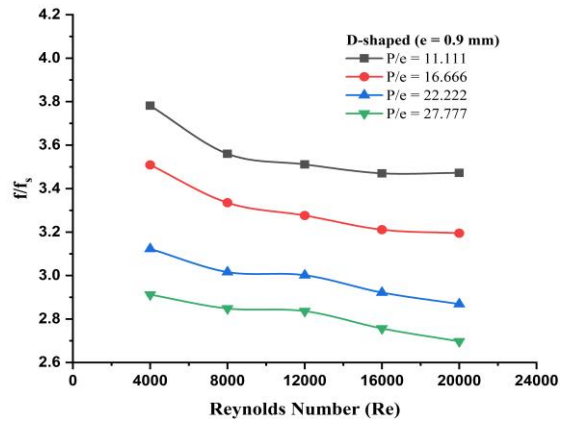
(b) D-shaped roughness

Figure 8. Variation of f with Re

Figure 9 (a), and (b) reveals that the ratio of the friction factor enhancement (f/f_s) decreases as the Re increases. Additionally, both configurations with higher P/e exhibit lower values of f/f_s . In cases where the relative roughness pitch is low, the absorber plate contains a higher number of ribs, resulting in more reattachment points. Consequently, low P/e arrangements experience a higher f/f_s due to the increased obstruction to flow caused by the present roughness. The maximum value of f/f_s was attained about 3.86 times and 3.47 times for B and D shape roughness respectively at P/e of 11.111 and Re of 4000.



(a) B-shaped roughness



(b) D-shaped roughness

Figure 9. Variation of f/f_s with Re

3.3.1. Effect of Roughness Shape Variation on Flow Characteristics

In this investigation, varied relative roughness pitch ($p/e = 11.11, 16.66, 22.22, 27.77$) and a constant relative roughness height ($D_h = 0.027$) have been utilized for all the examples using different levels of roughness on the absorber plate. D-shaped and B-shaped tabulators are the two types of tabulators that are used to create secondary flow and turbulence in the path of flowing fluid (air). Generally, roughness is used to create more turbulence by creating secondary flow, to break the laminar sublayer. The effects of secondary flow caused by different roughness geometry on turbulence creation and its impact on the laminar sub-layer have been extensively studied by various scholars. Arya et al. (2023), conducted a comparative study to analyze the combined effect of V-rib miniature with dimple roughness on performance and secondary flow generation in the SAH duct. The result reveals that the presence of a V-rib miniature upstream of the pure dimple generates complex secondary flow close to a wall. This configuration creates down-washing vortices, which strengthen the turbulent kinetic energy and flow mixing upstream of the dimple. As a result, there was an augmentation in heat transfer enhancement [81]. Further, this numerical investigation was extended by Arya et al. (2023), to analyze the performance of SAH and its effect on secondary flow using different types of miniature combined with dimple-shaped roughness. At a Re of 12,500, the peak THPP enhancement value of 1.63 has been observed in a dimple with a V-miniature at an angle of attack of 450 [82]. These studies have shed light on how the presence of roughness elements in the duct alters the flow patterns and enhances turbulence. The secondary flow generated by these roughness elements interacts with the main flow, leading to increased mixing and enhanced heat transfer. Researchers have found that the roughness elements induce vortices and swirling motion within the flow, promoting turbulence generation. These vortices disrupt the smooth flow and create eddies, resulting in intensified mixing and heat transfer enhancement. The turbulent flow caused by the secondary flow affects the laminar sub-layer, which is the thin layer near the duct wall characterized by low velocity and high viscous effects. The interaction between turbulence and the

laminar sub-layer alters the boundary layer dynamics, leading to changes in heat transfer characteristics. Different scholars have employed experimental, numerical, and analytical techniques to investigate the effects of roughened SAH duct on turbulence creation and the laminar sub-layer. Their findings provide valuable insights into the mechanisms behind enhanced heat transfer and contribute to the design and optimization of SAH ducts for improved performance in various applications.

The temperature, turbulent kinetic energy, and velocity contours are to be calculated for each scenario. For each example, variables like the Nusselt number and friction factor are to be determined. The comparison of outcomes will be done with those obtained using smooth ducts. In the end, the thermo-hydraulic performance factor will also be determined for each example by utilizing these values.

3.3.2. Velocity Contour

As a result, when ANSYS FLUENT has conducted the numerical analysis over the rectangular duct, velocity contour is received from it. This graph shows how the flow of air through the duct varies with velocity. The variance in velocity will be reduced when the smooth surface is used. However, the variance in velocity would be greater if there is some roughness inside the duct. This is because the area for air circulation below the ribs is limited, thus, to maintain a constant mass flow rate, the air velocity should rise below the ribs. The turbulence inside the duct will rise because of this increase in air velocity. The major purpose of adopting various roughness is to promote heat transfer between the absorber plate and the air, which will further result in this rise. However, it also has a drawback, which is an increase in pressure drop in the direction of flow. Therefore, to move the same amount of fluid, more force is needed.

Figure 10 (a), (b), (c), and (d) use a B-shaped roughness to show the fluctuation of velocity inside a flow duct. This graph is created using the Reynolds number of 18000. The 18000 Re number is used to compute the inlet velocity, which is 8.978m/s. Due to the no-slip condition, the absorber plate's minimum velocity is 0 m/s. 10.2184 m/s is the highest velocity that can be measured inside the duct. This is obtained at $p = 10m$. The figure shows velocity variation in different pitch distances.

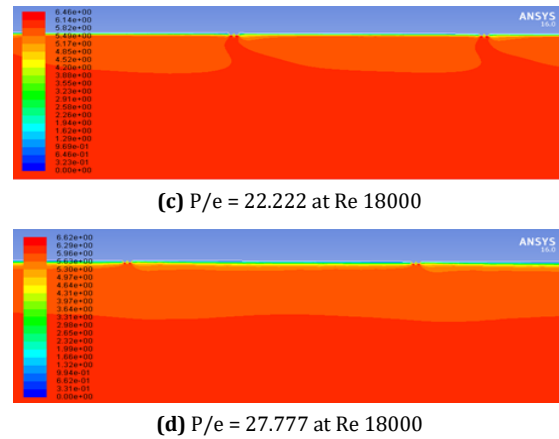
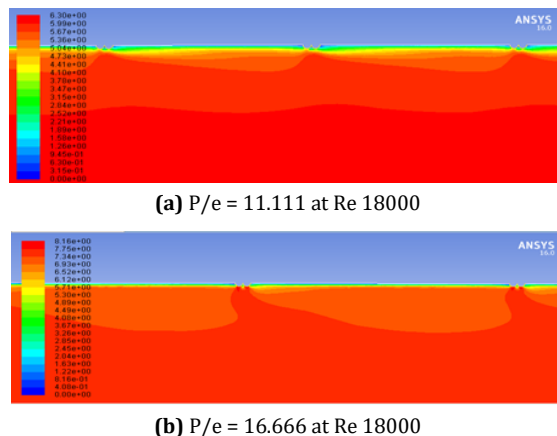


Figure 10. Velocity contours of B-shape roughened SAH at Re 18000

Figure 11 (a), (b), (c), and (d) use a D-shaped roughness to show the fluctuation of velocity inside a flow duct. This graph is created using the Reynolds number of 18000. The 18000 Re number is used to compute the inlet velocity, which is 8.878m/s. Due to the no-slip condition, the absorber plate's minimum velocity is 0 m/s. 10.1264 m/s is the highest velocity that can be measured inside the duct. This is obtained at a pitch distance of 10 mm. The figure shows velocity variation in different pitch distances.

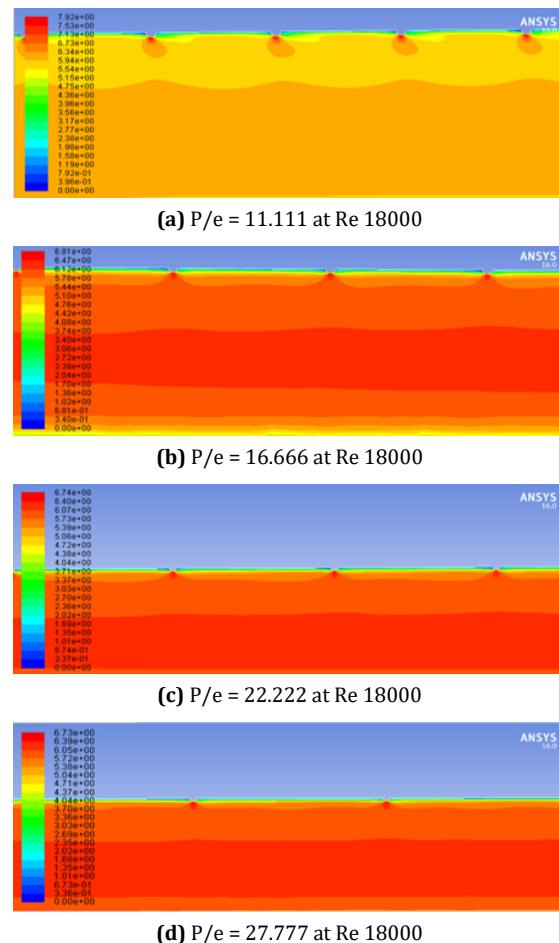


Figure 11. Velocity contours of D-shape roughened SAH at Re 18000

3.3.3. Turbulent Kinetic Energy Contour

The average kinetic energy per unit mass associated with eddies in turbulent flow is known as turbulent kinetic energy. Using turbulence kinetic energy, the intensity of turbulence in the flow field is directly expressed. Using turbulent kinetic energy contours, it is possible to comprehend the thermal phenomenon in an SAH that has been intentionally roughened. The contours demonstrate that the turbulent kinetic energy is at its highest close to the absorber plate and between the first and second ribs and that it diminishes as the absorber plate is approached farther.

In Figure 12 (a), (b), (c), and (d), B-shaped roughness is used to show the fluctuation of turbulent kinetic energy inside a flow duct with various pitch distances. This graph is created using the Reynolds number of 18000.

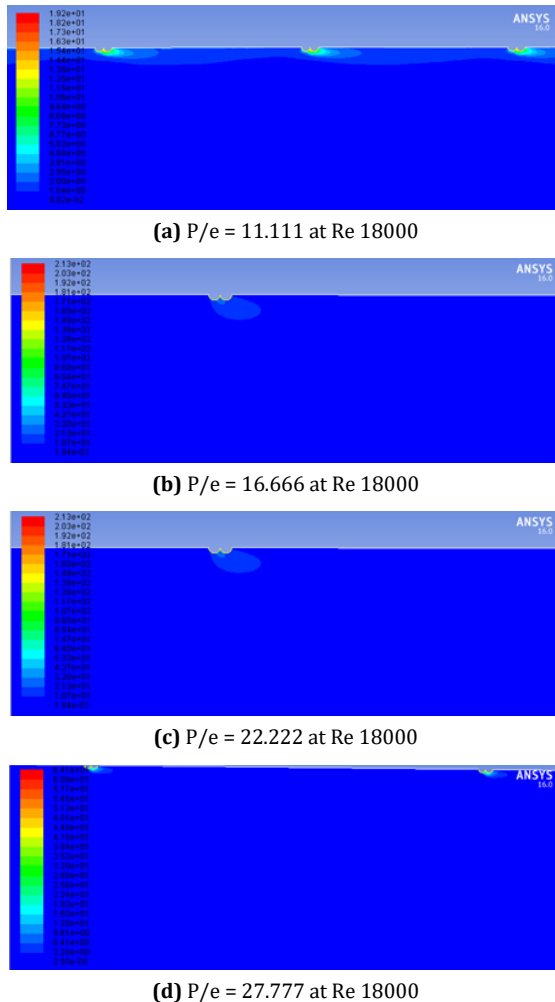


Figure 12. Velocity contours of B-shape roughened SAH at Re 18000

Figure 13 (a), (b), (c), (d) shows the variation of turbulence in D shape ribs varies p = 10cm, 15cm, 20cm, 25cm.

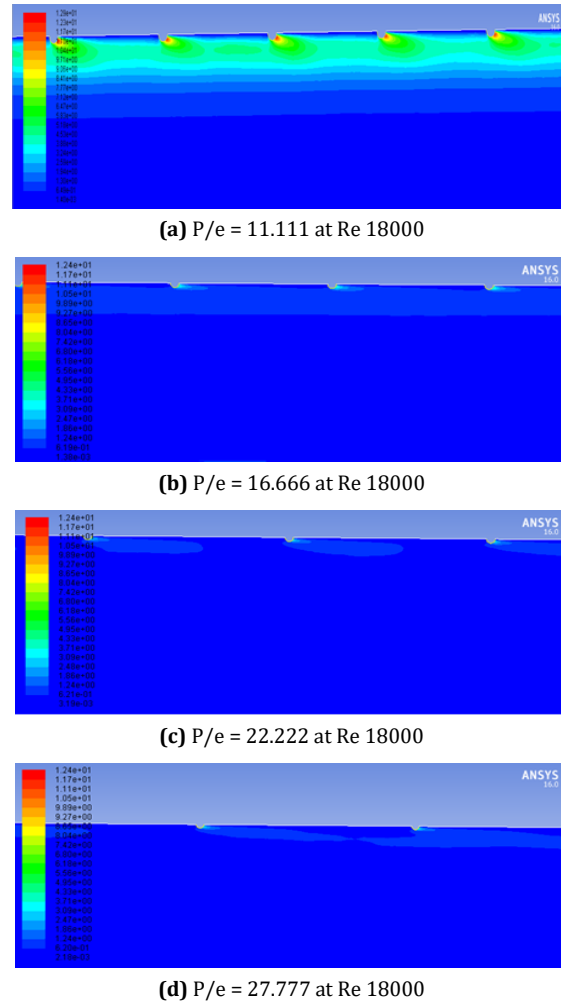


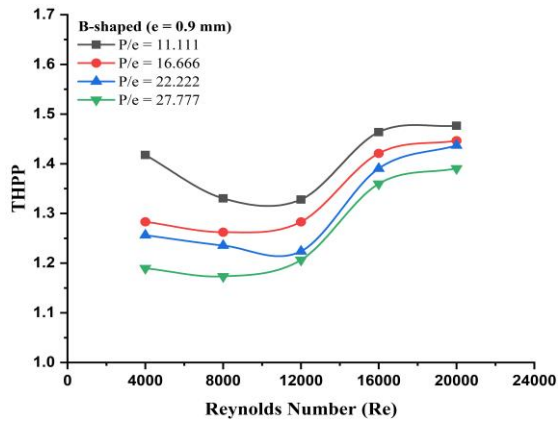
Figure 13. Velocity contours of D-shape roughened SAH at Re 18000

3.4. Effect on Thermohydraulic Performance Characteristics

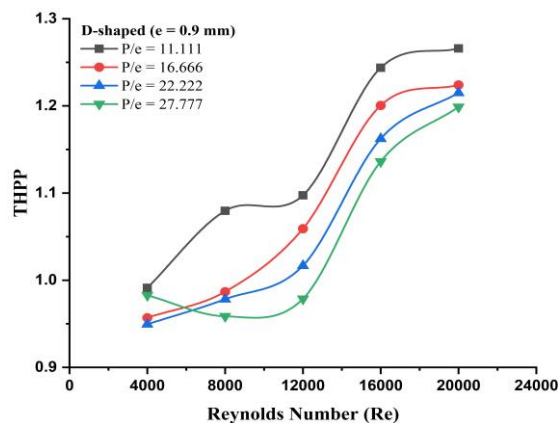
Thermo-hydraulic Performance Parameter (THPP) in the present numerical model of SAH roughened with B shape and D shape roughness was obtained by the correlation proposed by Webb and Eckert [89], and mathematically expressed in Eq. (8).

$$THPP = \frac{(N_u/Nu_s)}{(f/f_s)^{1/3}} \tag{8}$$

Figures 14 (a), and (b) illustrate the variation of THPP with Re for different P/e values at a constant e value of 0.9 mm. Figures show that increasing the Re improves the THPP of roughened SAH due to enhanced turbulence and increased heat transfer. The P/e, on the other hand, influences the intensity of flow disturbance and subsequent heat transfer enhancement, with lower pitch ratios typically resulting in higher heat transfer but also higher pressure drops. THPP increases with the increase in Re while starting to decrease with an increase in P/e values from 11.111 to 27.777. The analysis reveals that the optimum THPP is achieved at about 1.48, and 1.27 for B shape and D shape roughness respectively when P/e is approximately 11.111 (P = 10 mm) and Re of 20000.



(a) B- shaped roughness



(b) D- shaped roughness

Figure 14. Variation of THPP with Re

3.5. Comparison of the Present Study with Previous Experimental Data

To address and explain the novelty of the results obtained from the present numerical analysis of roughened SAH duct (with B shape roughness), the comparison has been made with existing research. The numerical results of Nu and f were compared with the previous study of square-sectioned transverse rib roughened SAH by Yadav et al. [90] under similar operating conditions. Figure 15 shows the comparison of Nu, and f corresponds to the Re for the present study and existing literature. Comparison results show that the present study provides superior heat transmission with 1.72% enhancement in Nu, and about 3.72% reduction in f for B shape roughness as compared to the square-sectioned ribs as roughness under similar operating conditions. Hence, the proposed model is quite better with higher Nu and offers lower frictional losses than the existing research.

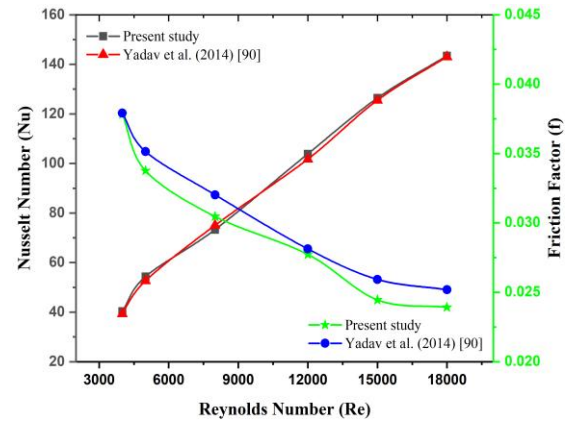


Figure 15. Comparison of Nu and f with previous research

4. Conclusions

The presented results pertain to a 2-D rectangular duct SAH equipped with a rough surface consisting of B-shaped and D-shaped ribs. The analysis focuses on examining the Nusselt number (Nu), Friction factor (f), and Thermohydraulic Performance Parameter (THPP) associated with these rib geometries within the rectangular duct. After analyzing the results, the following conclusions were drawn:

- The RNG $k-\epsilon$ model used in this study demonstrates good agreement with standard correlations, as it predicts Nu and f values closer to the correlations which provide credibility to the model.
- The highest value of Nu and f is observed at about 110.15 and 0.0386 for B shape roughness at P/e of 11.111 with a Re of 20000 and 4000 respectively.
- Significant improvement in the Nu and f enhancement ratios is observed 2.64 times and 3.869.15 times respectively for B shape roughness at P/e of 11.111 as compared to the smooth duct SAH.
- The highest peak THPP value of 1.47 is achieved for B-shape roughness at a P/e value of 11.111 (P = 10 mm), and e = 0.9 mm with a Reynolds number of 20000.
- The novelty of the B-shape and D-shape roughened SAH duct lies in their distinct roughness geometries, which set them apart from other roughness geometries.
- The shape of the geometry, along with different arrangements of pitch ratios, has a significant effect on flow characteristics and heat transfer in the SAH. Among the studied configurations (B shape and D shape), the B shape roughness yielded the highest THPP.

This numerical investigation successfully designs B-shaped and D-shaped ribs with different P/e in a rectangular duct SAH. Such SAHs can be employed in various applications, including drying (agricultural and industrial), timber seasoning, space heating, etc.

Further research could explore different modifications in roughness, such as varying the cross sections of the ribs or new geometries like C shape, R shape, etc., and to further enhance the performance of SAHs the investigation of hybrid roughness should be carried out in the following sub-areas:

1. Numerical and experimental investigation of thermal performance using different roughness under various arrangements of hybrid roughness.
2. A detailed study on exergy and entropy generation concept.

Nomenclature

SAH	Solar air heater
SPSAH	Single-pass solar air heater
DPSAH	Double-pass solar air heater
L	Length of duct [mm]
W	Width of rectangular duct [mm]
H	Height of rectangular duct [mm]
D_h	Hydraulic diameter of duct [mm]
e	Height of ribs [mm]
VG	Vortex generator
P	Pitch [mm]
δ'	Transition sub-layer thickness [mm]
T	Air temperature [K]
v	Air velocity [m/s]
W/H	Duct aspect ratio
Pr	Prandtl number
Re	Reynolds number
I	Uniform heat flux [W/m^2]
e/D_h	Relative roughness height
P/e	Relative roughness pitch
C _p	Specific heat [J/kgK]
k	Thermal conductivity of air [W/mK]
Nu	Nusselt number
f	Friction factor
ρ	The density of air [kg/m^3]
μ	The viscosity of air [kg/ms]

Acknowledgments

The authors are very grateful to Dr. Ajay Debbarma and Mr. Vijay Singh Bisht for their helpful discussions and suggestions.

Conflicts of Interest

The author declares that there is no conflict of interest regarding the publication of this manuscript. In addition, the authors have entirely observed the ethical issues, including plagiarism, informed consent, misconduct, data fabrication and/or falsification, double publication and/or submission, and redundancy.

References

- [1] Tsoutsos, T., Frantzeskaki, N. and Gekas, V., 2005. Environmental impacts from the solar energy technologies. *Energy Policy*, 33(3), pp.289–296. doi:[https://doi.org/10.1016/s03014215\(03\)00241-6](https://doi.org/10.1016/s03014215(03)00241-6).
- [2] Wang, Q. and Qiu, H. N., 2009. Situation and outlook of solar energy utilization in Tibet, China. *Renewable and Sustainable Energy Reviews*, 13(8), pp.2181–2186. doi:<https://doi.org/10.1016/j.rser.2009.03.011>.
- [3] Saidur, R., Islam, M.R., Rahim, N.A. and Solangi, K.H., 2010. A review on global wind energy policy. *Renewable and Sustainable Energy Reviews*, 14(7), pp.1744–1762. doi:<https://doi.org/10.1016/j.rser.2010.03.007>.
- [4] Goel, V., Hans, V.S., Singh, S., Kumar, R., Pathak, S.K., Singla, M., Bhattacharyya, S., Almatrafi, E., Gill, R.S. and Saini, R.P., 2021. A comprehensive study on the progressive development and applications of solar air heaters. *Solar Energy*, doi:<https://doi.org/10.1016/j.solener.2021.07.040>.
- [5] Dwivedi, A., Mishra, H., and Nagrath, V., 2021. A Review on Different Performance Enhancement Techniques for Solar Air Heaters. *Recent Advances in Mechanical Engineering: Select Proceedings of ITME 2019*, pp.1-9. DOI: 10.1007/978-981-15-8704-7_1.
- [6] Sharma, S.L. and Debbarma, A., 2022. A review on thermal performance and heat transfer augmentation in solar air heater. *International Journal of Sustainable Energy*, 41 (11), pp.1973-2019. <https://doi.org/10.1080/14786451.2022.2125518>.
- [7] Chaurasia, S., Goel, V. and Debbarma, A., 2023. Impact of hybrid roughness geometry on heat transfer augmentation in solar air heater: A review. *Solar Energy*. <https://doi.org/10.1016/j.solener.2023.02.052>.
- [8] Prasad, K. and Mullick, S.C., 1983. Heat transfer characteristics of a solar air heater used for drying purposes. *Applied Energy*, 13 (2), pp.83-93. [https://doi.org/10.1016/0306-2619\(83\)90001-6](https://doi.org/10.1016/0306-2619(83)90001-6).
- [9] Bopche, S.B. and Tandale, M.S. 2009. Experimental investigations on heat transfer and frictional characteristics of a turbulator roughened solar air heater duct. *International Journal of Heat and Mass Transfer*, 52 (11-12), pp.2834-2848. <https://doi.org/10.1016/j.ijheatmasstransfer.2008.09.039>.
- [10] Arulanandam, S.J., Hollands, K.T. and Brundrett, E., 1999. A CFD heat transfer analysis of the transpired solar collector under no-wind

- conditions. *Solar Energy*, 67 (1-3), pp.93-100. [https://doi.org/10.1016/S0038092X\(00\)00042-6](https://doi.org/10.1016/S0038092X(00)00042-6).
- [11] Chaube, A., Sahoo, P.K. and Solanki, S.C. 2006. Analysis of heat transfer augmentation and flow characteristics due to rib roughness over absorber plate of a solar air heater. *Renewable Energy*, 31 (3), pp.317-331. <https://doi.org/10.1016/j.renene.2005.01.012>.
- [12] Chaube, A., Sahoo, P.K. and Solanki, S.C., 2006. Effect of roughness shape on heat transfer and flow friction characteristics of solar air heater with roughened absorber plate. *WIT Transactions on Engineering Sciences*, 53, pp.43-51. doi:10.2495/HT060051.
- [13] Varol, Y. and Oztop, H.F., 2008. A comparative numerical study on natural convection in inclined wavy and flat-plate solar collectors. *Building and environment*, 43 (9), pp.1535-1544. <https://doi.org/10.1016/j.buildenv.2007.09.002>.
- [14] Kumar, S. and Saini, R.P., 2009. CFD based performance analysis of a solar air heater duct provided with artificial roughness. *Renewable energy*, 34 (5), pp.1285-1291. <https://doi.org/10.1016/j.renene.2008.09.015>.
- [15] Karmare, S.V. and Tikekar, A.N., 2010. Analysis of fluid flow and heat transfer in a rib grit roughened surface solar air heater using CFD. *Solar Energy*, 84 (3), pp.409-417. <https://doi.org/10.1016/j.solener.2009.12.011>.
- [16] Soi, A., Singh, R. and Bhushan, B., 2010. Effect of roughness element pitch on heat transfer and friction characteristics of artificially roughened solar air heater duct. *International Journal of Advanced Engineering Technology*, 1 (3), pp.339-346.
- [17] Rajput, R. S., Bhagoria, J. L., Giri, A. K., Kumar, A., 2010. Study of heat transfer and friction characteristic of various artificial roughness in solar air heater duct by using computational fluid dynamics (CFD) software. In: *Proceedings of international conference on advances in renewable energy*, June 2010.
- [18] Sharma, S., Singh, R. and Bhushan, B., 2011. CFD based investigation on effect of roughness element pitch on performance of artificially roughened duct used in solar air heaters. *International Journal of Advanced Engineering Technology*, 2 (1), pp.234-241.
- [19] Gawande, V.B., Dhoble, A.S., Zodpe, D.B., and Chamoli, S., 2016. A review of CFD methodology used in literature for predicting thermo-hydraulic performance of a roughened solar air heater. *Renewable and Sustainable Energy Reviews*, 54, pp.550-605. <https://doi.org/10.1016/j.rser.2015.10.025>.
- [20] Jhariya, K., Ranjan, R., and Paswan, M.K., 2015. A CFD based performance analysis of heat transfer enhancement in solar air heater provided with transverse semi-circular ribs. *International Journal of Innovative Research in science, Engineering and Technology*, 4, pp.4528-4537.
- [21] Kumar, K., Kaushik, S. and Bisht, V.S., 2017. CFD analysis on solar air heater with artificial roughened broken curved ribs. *International Journal of Scientific & Engineering Research*, 8, pp.264-275.
- [22] Bisht, N. and Bisht, V.S., 2018. CFD Analysis of Solar Air Heater Roughened With Crown Shape Roughness. *Asian Journal of Applied Science and Technology*, 2 (3), pp.73-82.
- [23] Ghildyal, A., Bisht, V.S., Bisht, A.S. and Kishor, K., 2020. Computational Fluid Dynamics Study of Roughened Solar Air Heater. *Advanced Science, Engineering and Medicine*, 12(11), pp.1408-1411. <https://doi.org/10.1166/asem.2020.2595>.
- [24] Bisht, V.S., Patil, A.K. and Gupta, A., 2020. Thermo-Hydraulic Performance of Solar Air Heater Roughened with V-Shaped Ribs Combined with V-Shaped Perforated Baffles. In *Advances in Energy Research, Vol. 2: Selected Papers from ICAER 2017, Springer Singapore*, pp. 123-132. DOI: 10.1007/978-981-15-2662-6_12.
- [25] Bahuguna, R., Chamoli, S., Barthwal, Y., Rana, S., Gupta, A., and Bisht, V.S., 2022. Economic analysis of artificially roughened solar air heater with v-shaped ribs. *Acta Innovations*, 44, pp.18-33. <https://doi.org/10.32933/ActaInnovations.44.2>
- [26] Bahuguna, R., Mer, K.K.S., Kumar, M., Chamoli, S., 2021. Thermohydraulic performance and second law analysis of a tube embedded with multiple helical tape inserts. *Energy Sources, Part A: Recovery, Utilization, and Environmental Effects*, pp.1-23. <https://doi.org/10.1080/15567036.2021.1904057>.
- [27] Chamoli, S., Lu, R., Jin Xie, J., and Yu, P., 2018. Numerical Study on Flow Structure and Heat Transfer in a Circular Tube Integrated with Novel Anchor Shaped Inserts. *Applied Thermal Engineering*, 135, pp.304-24. <https://doi.org/10.1016/j.applthermaleng.2018.02.052>.
- [28] Bahuguna, R., Mer, K.K.S., Kumar, M., Chamoli, S., 2021. Entropy generation analysis in a tube heat exchanger integrated with triple blade vortex generator inserts. *Energy Sources, Part A: Recovery, Utilization, and Environmental Effects*, pp.1-19. <https://doi.org/10.1080/15567036.2021.1918291>.
- [29] Maithani, R. and Kumar, A., 2020. Correlations Development for Nusselt Number and Friction Factor in a Dimpled Surface Heat Exchanger Tube. *Experimental Heat Transfer*, 33 (2), pp.101-22. <https://doi.org/10.1080/08916152.2019.1573863>.
- [30] Bahuguna, R., Mer, K.K.S., Kumar, M., Chamoli, S. (2022). Thermal performance of a circular tube embedded with TBVG inserts: an experimental study. *Journal of Thermal Analysis and Calorimetry*, 147(20), pp.11373-11389. <https://doi.org/10.1007/s10973-022-11352-1>.
- [31] Singh, V. P., Jain, S. and Gupta, J.M.L., 2023. Analysis of the effect of perforation in multi-v rib artificial roughened single pass solar air heater: - Part A. *Experimental Heat Transfer*, 36(2), 163-182. <https://doi.org/10.1080/08916152.2021.1988761>.
- [32] Singh, V. P., Jain, S. and Gupta, J.M.L., 2022. Analysis of the effect of variation in open area

- ratio in perforated multi-V rib roughened single pass solar air heater-Part A. *Energy sources, part a: recovery, utilization, and environmental effects*, pp.1-21. <https://doi.org/10.1080/15567036.2022.2029976>.
- [33] Singh, V. P., Jain, S. and Gupta, J.M.L., 2022. Performance assessment of double-pass parallel flow solar air heater with perforated multi-V ribs roughness—Part B. *Experimental Heat Transfer*, 35(7), pp.1059-1076. <https://doi.org/10.1080/08916152.2021.2019147>.
- [34] Singh, V. P., Jain, S., Karn, A., Dwivedi, G., Kumar, A., Mishra, S. and Kamel, S., 2022. Heat transfer and friction factor correlations development for double pass solar air heater artificially roughened with perforated multi-V ribs. *Case Studies in Thermal Engineering*, 39, pp.102461. <https://doi.org/10.1016/j.csite.2022.102461>.
- [35] Sarreshtedari, A. and Zamani Aghaee, A., 2014. Investigation of the thermo-hydraulic behavior of the fluid flow over a square ribbed channel. *Journal of Heat and Mass Transfer Research*, 1(2), pp.101-106.
- [36] Noghrehabadi, A., Hajidavalloo, E. and Moravej, M., 2016. An experimental investigation of performance of a 3-D solar conical collector at different flow rates. *Journal of Heat and Mass Transfer Research*, 3(1), pp.57-66.
- [37] Gupta, N.K. and Alam, T., 2021. A review on augmentation in thermal performance of solar water heater using phase change material. In *IOP Conference Series: Materials Science and Engineering*, 1116 (1), pp.012075. IOP Publishing. DOI 10.1088/1757-899X/1116/1/012075.
- [38] Gupta, N. K. and Alam, T., 2021. A Review on Augmentation in Thermal Performance of Solar Air Heater. In *IOP Conference Series: Materials Science and Engineering*, 1116 (1), pp. 012064. IOP Publishing. DOI 10.1088/1757-899X/1116/1/012064.
- [39] Karmveer, Gupta, N.K., Alam, T., Cozzolino, R. and Bella, G., 2022. A descriptive review to access the most suitable rib's configuration of roughness for the maximum performance of solar air heater. *Energies*, 15(8), pp.2800. <https://doi.org/10.3390/en15082800>.
- [40] Karmveer, Gupta, N.K., Siddiqui, M.I.H., Dobrotă, D., Alam, T., Ali, M.A. and Orfi, J., 2022. The effect of roughness in absorbing materials on solar air heater performance. *Materials*, 15 (9), pp.3088. <https://doi.org/10.3390/ma15093088>.
- [41] Karmveer, Gupta, N.K., Alam, T. and Singh, H., 2022. An Experimental Study of Thermohydraulic Performance of Solar Air Heater Having Multiple Open Trapezoidal Rib Roughnesses. *Experimental Heat Transfer*, pp.1-21. <https://doi.org/10.1080/08916152.2022.2139024>.
- [42] Gupta, N. K. and Alam, T., 2023. Experimental investigation of thermohydraulic performance of solar thermal collector for sustainable built environment. *Sustainable Energy Technologies and Assessments*, 57, pp.103257. <https://doi.org/10.1016/j.seta.2023.103257>.
- [43] Karmveer, Gupta, N.K. and Alam, T., 2023. Development of correlations for predicting Nusselt number and friction factor of roughened solar air heater duct for sustainable development. *Experimental Heat Transfer*, pp.1-19. <https://doi.org/10.1080/08916152.2023.2189329>.
- [44] Gupta, N. K. and Alam, T., 2023. Effect of relative rib roughness pitch on the thermohydraulic performance of roughened duct of solar air heater. *Materials Today: Proceedings*. <https://doi.org/10.1016/j.matpr.2023.01.310>.
- [45] Bhushan, B. and Singh, R., 2011. Nusselt number and friction factor correlations for solar air heater duct having artificially roughened absorber plate. *Solar energy*, 85(5), pp.1109-1118. <https://doi.org/10.1016/j.solener.2011.03.007>.
- [46] Lanjewar, A., Bhagoria, J.L. and Sarviya, R.M., 2011a. Experimental study of augmented heat transfer and friction in solar air heater with different orientations of W-Rib roughness. *Experimental Thermal and Fluid Science*, 35(6), pp.986-995. <https://doi.org/10.1016/j.expthermflusci.2011.01.019>.
- [47] Lanjewar, A., Bhagoria, J.L. and Sarviya, R.M., 2011b. Heat transfer and friction in solar air heater duct with W-shaped rib roughness on absorber plate. *Energy*, 36(7), pp.4531-4541. <https://doi.org/10.1016/j.energy.2011.03.054>.
- [48] Kumar, A., Saini, R.P. and Saini, J.S., 2012. Experimental investigation on heat transfer and fluid flow characteristics of air flow in a rectangular duct with Multi v-shaped rib with gap roughness on the heated plate. *Solar Energy*, 86(6), pp.1733-1749. <https://doi.org/10.1016/j.solener.2012.03.014>.
- [49] Yadav, S. and Kaushal, M., 2013. Nusselt number and friction factor correlations for solar air heater duct having protrusions as roughness elements on absorber plate. *Experimental Thermal and Fluid Science*, 44, pp.34-41. <https://doi.org/10.1016/j.expthermflusci.2012.05.011>.
- [50] Karwa, R. and Chitoshiya, G., 2013. Performance study of solar air heater having v-down discrete ribs on absorber plate. *Energy*, 55, pp.939-955. <https://doi.org/10.1016/j.energy.2013.03.068>.
- [51] Singh, A.P., 2014. Heat transfer and friction factor correlations for multiple arc shape roughness elements on the absorber plate used in solar air heaters. *Experimental Thermal and Fluid Science*, 54, pp.117-126. [10.1016/j.expthermflusci.2014.02.004](https://doi.org/10.1016/j.expthermflusci.2014.02.004).
- [52] Yadav, A. S. and Bhagoria, J.L., 2014. A CFD based thermo-hydraulic performance analysis of an artificially roughened solar air heater having equilateral triangular sectioned rib roughness on the absorber plate. *International Journal of Heat and Mass Transfer*, 70, pp.1016-1039. <https://doi.org/10.1016/j.ijheatmasstransfer.2013.11.074>.
- [53] Maithani, R. and Saini, J.S., 2017. Performance evaluation of solar air heater having V-ribs with symmetrical gaps in a rectangular duct of solar air heater. *International Journal of Ambient*

- Energy*, 38(4), pp.400-410. <https://doi.org/10.1080/01430750.2015.1133455>.
- [54] Pandey, N. K., Bajpai, V. K. and Varun, 2016. Heat transfer and friction factor study of a solar air heater having multiple arcs with gap-shaped roughness element on absorber plate. *Arabian Journal for Science and Engineering*, 41(11), pp.4517-4530. [10.1007/s13369-016-2148-9](https://doi.org/10.1007/s13369-016-2148-9).
- [55] Gawande, V. B., Dhoble, A.S., Zodpe, D.B. and Chamoli, S., 2016a. Analytical approach for evaluation of thermo hydraulic performance of roughened solar air heater. *Case Studies in Thermal Engineering*, 8, pp.19-31. <https://doi.org/10.1016/j.csite.2016.03.003>.
- [56] Gawande, V.B., Dhoble, A.S., Zodpe, D.B. and Chamoli, S., 2016. Experimental and CFD-based thermal performance prediction of solar air heater provided with chamfered square rib as artificial roughness. *Journal of the Brazilian Society of Mechanical Sciences and Engineering*, 38 (2), pp.643-663. <https://doi.org/10.1007/s40430-015-0402-9>.
- [57] Bharadwaj, G., Varun, Kumar, R. and Sharma, A., 2017. Heat transfer augmentation and flow characteristics in ribbed triangular duct solar air heater: An experimental analysis. *International journal of green energy*, 14(7), pp.587-598. <https://doi.org/10.1080/15435075.2017.1307751>.
- [58] Sawhney, J.S., Maithani, R. and Chamoli, S., 2017. Experimental investigation of heat transfer and friction factor characteristics of solar air heater using wavy delta winglets. *Applied thermal engineering*, 117, pp.740-751. <https://doi.org/10.1016/j.applthermaleng.2017.01.113>.
- [59] Gabhane, M.G. and Kanase-Patil, A.B., 2017. Experimental analysis of double flow solar air heater with multiple C shape roughness. *Solar Energy*, 155, pp.1411-1416. <https://doi.org/10.1016/j.solener.2017.07.038>.
- [60] Kumar, R., Kumar, A. and Goel, V., 2017b. A parametric analysis of rectangular rib roughened triangular duct solar air heater using computational fluid dynamics. *Solar Energy*, 157, pp.1095-1107. <https://doi.org/10.1016/j.solener.2017.08.071>.
- [61] Alam, T. and Kim, M.H., 2017. Heat transfer enhancement in solar air heater duct with conical protrusion roughness ribs. *Applied Thermal Engineering*, 126, pp.458-469. <https://doi.org/10.1016/j.applthermaleng.2017.07.181>.
- [62] Thakur, D.S., Khan, M.K. and Pathak, M., 2017. Solar air heater with hyperbolic ribs: 3D simulation with experimental validation. *Renewable Energy*, 113, pp.357-368. <https://doi.org/10.1016/j.renene.2017.05.096>.
- [63] Singh, I. and Singh, S., 2018. CFD analysis of solar air heater duct having square wave profiled transverse ribs as roughness elements. *Solar Energy*, 162, pp.442-453. [10.1016/j.solener.2018.01.019](https://doi.org/10.1016/j.solener.2018.01.019).
- [64] Kumar, A. and Layek, A., 2018. Thermo-hydraulic performance of solar air heater having twisted rib over the absorber plate. *International Journal of Thermal Sciences*, 133, pp.181-195. <https://doi.org/10.1016/j.ijthermalsci.2018.07.026>.
- [65] Soi, A., Singh, R. and Bhushan, B., 2018. Heat transfer and friction characteristics of solar air heater duct having protruded roughness geometry on absorber plate. *Experimental Heat Transfer*, 31(6), pp.571-585. <https://doi.org/10.1080/08916152.2018.1468832>.
- [66] Abuşka, M., 2018. Energy and exergy analysis of solar air heater having new design absorber plate with conical surface. *Applied Thermal Engineering*, 131, pp.115-124. <https://doi.org/10.1016/j.applthermaleng.2017.11.129>.
- [67] Debnath, S., Das, B. and Randive, P., 2019. Influences of pentagonal ribs on the performance of rectangular solar air collector. *Energy Procedia*, 158, pp.1168-1173. <https://doi.org/10.1016/j.egypro.2019.01.300>.
- [68] Singh, I., Vardhan, S., Singh, S. and Singh, A., 2019. Experimental and CFD analysis of solar air heater duct roughened with multiple broken transverse ribs: A comparative study. *Solar Energy*, 188, pp.519-532. <https://doi.org/10.1016/j.solener.2019.06.022>.
- [69] Bezbaruah, P.J., Das, R.S. and Sarkar, B.K., 2019. Thermo-hydraulic performance augmentation of solar air duct using modified forms of conical vortex generators. *Heat and Mass Transfer*, 55 (5), pp.1387-1403. <https://doi.org/10.1007/s00231-018-2521-1>.
- [70] Kumar, R., Goel, V., Singh, P., Saxena, A., Kashyap, A. S. and Rai, A., 2019. Performance evaluation and optimization of solar assisted air heater with discrete multiple arc shaped ribs. *Journal of Energy Storage*, 26, pp.100978. <https://doi.org/10.1016/j.est.2019.100978>.
- [71] Wang, D., Liu, J., Liu, Y., Wang, Y., Li, B. and Liu, J., 2020. Evaluation of the performance of an improved solar air heater with "S" shaped ribs with gap. *Solar Energy*, 195 (13), pp.89-101. <https://doi.org/10.1016/j.solener.2019.11.034>.
- [72] Kumar, R., Kashyap, A. S., Singh, P., Goel, V. and Kumar, K., 2020. Innovatively arranged curved-ribbed solar-assisted air heater: performance and correlation development for heat and flow characteristics. *Journal of Solar Energy Engineering*, 142(3), pp.031011. <https://doi.org/10.1115/1.4045827>.
- [73] Ahmad, I., Khan, N.H., Hassan, M.A. and Paswan, M.K., 2020. Three-dimensional thermo-hydraulic analysis of solar air heater with equilateral prism-shaped rib roughness. *Journal of Solar Energy Engineering*, 142(5), pp.051001. <https://doi.org/10.1115/1.4046088>.
- [74] Ngo, T.T. and Phu, N.M., 2020. Computational fluid dynamics analysis of the heat transfer and pressure drop of solar air heater with conic-curve profile rib. *Journal of Thermal Analysis and Calorimetry*, 139 (5), pp.3235-3246. <https://doi.org/10.1007/s10973-019-08709-4>.
- [75] Rathor, Y. and Aharwal, K.R., 2020. Heat transfer enhancement due to a staggered element using liquid crystal thermography in an inclined discrete rib roughened solar air

- heater. *International Communications in Heat and Mass Transfer*, 118, pp.104839. <https://doi.org/10.1016/j.icheatmasstransfer.2020.104839>.
- [76] Mahanand, Y. and Senapati, J.R., 2020. Thermal enhancement study of a transverse inverted-T shaped ribbed solar air heater. *International Communications in Heat and Mass Transfer*, 119, pp.104922. <https://doi.org/10.1016/j.icheatmasstransfer.2020.104922>.
- [77] Mahanand, Y. and Senapati, J.R., 2021. Thermo-hydraulic performance analysis of a solar air heater (SAH) with quarter-circular ribs on the absorber plate: A comparative study. *International Journal of Thermal Sciences*, 161, pp.106747. <https://doi.org/10.1016/j.ijthermalsci.2020.106747>.
- [78] Jain, S.K., Agrawal, G.D. and Misra, R., 2021. Heat transfer augmentation using multiple gaps in arc-shaped ribs roughened solar air heater: An experimental study. *Energy Sources, Part A: Recovery, Utilization, and Environmental Effects*, 43(24), pp.3345-3356. <https://doi.org/10.1080/15567036.2019.1607945>.
- [79] Azad, R., Bhuvad, S. and Lanjewar, A., 2021. Study of solar air heater with discrete arc ribs geometry: Experimental and numerical approach. *International Journal of Thermal Sciences*, 167, pp.107013. <https://doi.org/10.1016/j.ijthermalsci.2021.107013>.
- [80] Bhuvad, S.S., Azad, R. and Lanjewar, A., 2022. Thermal performance analysis of apex-up discrete arc ribs solar air heater-an experimental study. *Renewable Energy*, 185, pp.403-415. <https://doi.org/10.1016/j.renene.2021.12.037>.
- [81] Arya, N. and Goel, V., 2023. Comparative study of V-ribs miniature with dimple hybrid roughness along with dimples shaped roughness used in solar air heating system. *Energy Sources, Part A: Recovery, Utilization, and Environmental Effects*, 45(2), pp.3297-3317. <https://doi.org/10.1080/15567036.2023.2195822>.
- [82] Arya, N. Goel, V. and Sunden, B., 2023. Solar air heater performance enhancement with differently shaped miniature combined with dimple shaped roughness: CFD and experimental analysis. *Solar Energy*, 250, pp.33-50. <https://doi.org/10.1016/j.solener.2022.12.024>.
- [83] Wood, J.N., De Nayer, G., Schmidt, S. and Breuer, M., 2016. Experimental investigation and large-eddy simulation of the turbulent flow past a smooth and rigid hemisphere. *Flow, Turbulence and Combustion*, 97, pp.79-119. doi:10.1007/s10494-015-9690-5.
- [84] Chaube, A., Sahoo, P.K. and Solanki, S.C., 2006. Analysis of heat transfer augmentation and flow characteristics due to rib roughness over absorber plate of a solar air heater. *Renewable Energy*, 31(3), pp.317-331. <https://doi.org/10.1016/j.renene.2005.01.012>.
- [85] Standard, A.S.H.R.A.E., 1977. Methods of testing to determine the thermal performance of solar collectors. *American Society of Heating*, 93-77.
- [86] Verma, S.K. and Prasad, B.N., 2000. Investigation for the optimal thermohydraulic performance of artificially roughened solar air heaters. *Renewable Energy*, 20(1), pp.19-36. [https://doi.org/10.1016/S09601481\(99\)00081-6](https://doi.org/10.1016/S09601481(99)00081-6).
- [87] Kays, W.M., 1985. Forced convection, internal flow in ducts. *Handbook of heat transfer fundamentals*. <https://cir.nii.ac.jp/crid/1570291225769794304.bib?lang=ja>.
- [88] Bhatti, M.S., 1987. Turbulent and transition flow convective heat transfer in ducts. *Handbook of single-phase convective heat transfer*. <https://cir.nii.ac.jp/crid/1573387448915440896.bib?lang=ja>.
- [89] Webb, R.L. and Eckert, E.R.G., 1972. Application of rough surfaces to heat exchanger design. *International Journal of Heat and Mass Transfer*, 15, pp.647-1658, [https://doi.org/10.1016/0017-9310\(72\)90095-6](https://doi.org/10.1016/0017-9310(72)90095-6).
- [90] Yadav, A.S. and Bhagoria, J.L., 2014. A numerical investigation of square sectioned transverse rib roughened solar air heater. *International Journal of Thermal Sciences*, 79, pp.111-131. <https://doi.org/10.1016/j.ijthermalsci.2014.01.008>.